Resilience-oriented optimal post-disruption reconfiguration for coupled traffic-power systems

Hongping Wang, Yi-Ping Fang, Enrico Zio

Version of Record: https://www.sciencedirect.com/science/article/pii/S0951832022000801
Manuscript_98fb680d652a1d1408840d83f7450409

Resilience-oriented optimal post-disruption reconfiguration for coupled traffic-power systems

Hongping Wang[a,b], Yi-Ping Fang[b,*], Enrico Zio[c,d]

[a]*School of modern post (School of automation), Beijing University of Posts and Telecommunications, Beijing, China*
[b]*Université Paris-Saclay, CentraleSupélec, Laboratoire Génie Industriel, 3 rue Joliot-Curie, Gif-sur-Yvette, France.*
[c]*Energy Department, Politecnico di Milano, 20156 Milano, Italy.*
[d]*Mines ParisTech, PSL Research University, CRC, Sophia Antipolis, France.*

Abstract

The increasing penetration of grid-enabled electric vehicles (EVs) renders road networks (RNs) and power networks (PNs) increasingly interdependent for normal operation. For this reason, recently few studies have started to investigate the vulnerability of a highly coupled traffic-power system in the presence of disruptive events. Actually, however, only very few of these studies have considered the impact of EVs on the interdependent traffic-power system during restoration from a disruptive event. In an attempt to fill this gap, in this study, we investigate the restoration planning of both independent RNs and PNs, and interdependent traffic-power systems. A mixed integer program model is formulated to provide optimal reconfiguration and operational solutions for post-disruption traffic-power systems recovery. The objective of the model is to minimize the total cost incurred by system performance loss, which is quantified by the cumulative unmet traffic demand for RNs and load shedding cost for PNs. Several reconfiguration strategies are considered, including links reversing in RNs and line switching in PNs, to optimize system resilience. In the proposed model, the integrated problem of system optimal dynamic traffic assignment and optimal power flow is solved to derive the optimal traffic-power flow. RNs and PNs are coupled through the coordinately allocated spatio-temporal charging demand of EVs. A partial highway network in North Carolina (NC), USA, and a modified IEEE-14 bus system are used to illustrate the application of the model. The numerical results obtained show the added value of coordinately planning restoration for traffic-power systems and the effects of different levels of EV penetration.

Keywords: Interdependent systems, Traffic-power systems, Electric vehicles, Resilience, Fast-charging stations, Optimal traffic-power flow

Acronyms

EVs	Electric vehicles
GVs	Gasoline vehicles
RNs	Road networks
PNs	Power networks
FCSs	Fast-charging stations

Nomenclature

*Corresponding author, Email address: yiping.fang@centralesupelec.fr

Indices

a	index of links
t	index of periods
s	index of destinations
e	index of energy levels for EVs
c	index of EV classes

The transportation network sets

$\mathcal{A}$	set of arcs
$\mathcal{N}$	set of nodes
$\mathcal{N}_{SR}$	set of origin and destination nodes
$A(i)(B(i))$	set of links whose tail(head) node is i
$\mathcal{A}_R$	set of source arcs
$\mathcal{A}_S$	set of sink arcs
$\mathcal{A}_G$	set of general arcs
$\mathcal{A}_C$	set of charging arcs
$\mathcal{T}$	set of periods
$\mathcal{E}_c$	set of energy levels for the EVs belonging to class c
$\mathcal{C}$	set of EV classes

Parameters

ϕ	time value
p_a^{ev}	charging power of charging link a
$NC_a(t)$	number of chargers at charging link a during period t
δ	period length
L_a	physical length of link a
$k_{jam}/q_{max}/v_f$	jam density/ maximum flow/ free-flow speed
w	backward shock-wave speed, $w = q_{max} \cdot v_f/(q_{max} - k_{jam} \cdot v_f)$
α_a^t	average charging speed for charging link a during period t, $\alpha_a^t = p_a^{ev}/(\eta \cdot v_f)$
$f_a^I(t)$	inflow capacity of link a during period t

$f_a^O(t)$ outflow capacity of link a during period t

$DG_a^s(t)$ cumulative gasoline vehicle travel demand between the entry of origin link a and destination s, at the end of period t

$DE_{a,c}^{s,e}(t)$ cumulative electric power travel demand of c class EV between the entry of origin link a and destination s with energy level e at the end of period t

ν_a free-flow travel time on link a, $\nu_a = L_a/(\delta \cdot v_f)$

β_a travel time required by the backward shock wave from the exit to the entry of link a, $\beta_a = L_a/(\delta \cdot w)$

N_h number of links that can be reversed during restoration

Variables

$U_a(t)$ cumulative number of vehicles that enter link a by the end of period t

$V_a(t)$ cumulative number of vehicles that leave link a by the end of period t

$UG_a^s(t)$ cumulative number of GVs that enter link a to destination s by the end of period t

$VG_a^s(t)$ cumulative number of GVs that leave link a to destination s by the end of period t

$UE_{a,c}^{s,e}(t)$ cumulative number of EVs of class c with energy level e that enter link a to destination s by the end of period t

$VE_{a,c}^{s,e}(t)$ cumulative number of EVs of class c with energy level e that leave link a to destination s by the end of period t

$x_{a,c}^{s,e}(t)$ occupancy of EVs of class c with energy level e at charging link a during period t

$\hat{x}_{a,c}^{s,e}(t)$ occupancy of EVs of class c with the **updated** energy level e at charging link a during period t

h_a binary variable that is equal to 1 if the direction of road a is reversed, and 0 otherwise

The power network sets

$\mathcal{P}_N$ set of buses

$\mathcal{P}_L$ set of transmission lines

$\widetilde{\mathcal{P}}_L$ set of damaged transmission lines

$\Gamma(j)$ successor set of bus j

Parameters

p_j^{ramp} ramp limits of generators at bus j

c_j^b load shedding cost for the base load at bus j

c_j^{dc} load shedding cost for the EV charging load at bus j

$\underline{p}_j^g/\overline{p}_j^g$	lower/upper limit of power generation at bus j
$p_{j,t}^b$	base power demand at bus j during period t
N_u	number of lines that can be switched off during restoration

Variables

$p_{j,t}^g$	power generation at bus j during period t
$p_{j,t}^{dc}$	charging load at bus j during period t
$P_{i,j,t}$	power flow from bus i to j during period t
$\theta_{i,t}$	phase angle at bus i during period t
$u_{i,j}$	binary variable that is equal to 1 if line (i,j) is switched in, being 0 otherwise
$LS_{j,t}^{dc}$	binary variable that is equal to 1 if the load of the attached FCSs is shedded at bus j during period t, being 0 otherwise
$LS_{j,t}^b$	base load shedding at bus j during period t

EVs

Parameters

L_c^{max}	mileage of c class EV
E_c	maximum energy level of c class EV
η	average energy consumption efficiency for EVs

1. Introduction

Road networks (RNs) and power networks (PNs) are becoming increasingly interdependent due to the increasing penetrations of grid-enabled electric vehicles (EVs). Such increased interdependence makes the resulting system of systems more vulnerable also to the negative effects of technology-nature and human-caused incidents and accidents. In particular, when a high-impact low-probability (HILP) event occurs, e.g., an earthquake, an hurricane, a flood due to heavy rain, the consequences can be devastating. For example, the 2003 North America blackout caused 50 million customers to suffer power outage [1]; during the landfall of Hurricane Sandy in 2012, 65% of New Jersey's residents experienced disconnections from the power systems [2]; in July 2021, the extremely heavy rainfall caused city-wide floods in Zhengzhou, Henan province, China [3] and the flood severely damaged the critical infrastructures, including the transportation and the power systems, for an estimated direct economic loss on the order of RMB 88.5 billion. These examples highlight the pressing need of strengthening the resilience of RNs and PNs, also in view of the increasing frequency and intensely of these events.

The concept of resilience has emerged in recent years, but it is not a completely new concept and has strong relationships with the concepts of safety and risk. Resilience has various definitions [4, 5, 6, 7], most sharing the general idea that is relates to the ability of a system to prepare for, absorb, recover from and adapt to disturbances [8]. The risk concept concerns the threat of

an event to a system and its likelihood (probability) of occurrence and consequences, with less emphasis on the system recovery ability. As for the concept safety, Aven [9] pointed out that it has three perspectives:

- Safety I focuses on that things go wrong because of identifiable malfunctions or failures of specific components of the system;
- Safety II is seen as the ability to succeed under varying conditions;
- Safety III is defined as freedom from unacceptable losses.

The concept of resilience somewhat combines Safety I and II, whereas Safety III emphasizes that the system must be designed to be resilient and flexible to deal with surprising or unexpected events [10]. Resilience management plays a critical role in risk management [11]. Improved system resilience also means reduced risks [9].

From the definition of resilience, we can see that restoration ability is a key element. Effective restoration strategies are crucial to enhance the system's resilience to disruptions. The restoration problems can be generally divided into two stages: the long-term restoration problem and the short-term restoration problem. For the long-term restoration, the restoration duration could be days or weeks. For the PNs, it could be days, whereas it could be weeks for the RNs. During long-term restoration, the main target is to repair the physically damaged system components (e.g., transmission lines, road sections and generation stations) in order to recover the system performance to the pre-disruption level. Scheduling repair crews, allocating resources and determining the restoration priority of components are generally the major concerns for the long-term restoration problem. On the other hand, short-term restoration problem is also usually formed as emergency response problem, which aims at minimizing the system service degradation, maintaining the system service as much as possible, and trying to partially recover the disrupted service. Such kind of emergency response is carried out based on the available resources within hours after the disruption. The long-term and short-term restoration problems are conventionally treated separately, because there is no strong coupling relationship between them and they are different in terms of required resources, time scales, expected achievements, etc.

Many studies [12, 13, 14] have investigated the post-disruption optimal restoration of RNs and PNs.

Some studies [15, 16] treat the PN as an independent system. In these studies, restoration strategies, such as topology control [17], generator rescheduling [18, 19] and control of distributed energy storage systems, are often discussed. Among them, topology control is one of the most efficient strategies to restore the service and to enhance the system resilience. Switching operations has been intensively investigated [20, 21, 22] in PNs. In analogy to Braess's paradox in RNs Braess [23], Zhang et al. [17], Glavitsch [24] showed that if one transmission line is removed from the an electric power system, it can:

- enhance or reduce existing line currents,
- increase or decrease the losses in the neighboring lines,
- increase or decrease the magnitude of the nodal voltages.

Therefore, if the switching operations are optimized sophistically and applied correctly, it is clear that the control can be oriented towards overload reduction, control of voltage magnitudes and reduction of losses and short-circuit currents. Typically, maximizing the network resilience and

minimizing the number of switching operations are the objectives of the proposed optimization models. For example, Sekhavatmanesh and Cherkaoui [25] developed the concept of multiagent automation in smart grids to restore a maximum of loads with minimum switching operations after disruptions; Sabouhi et al. [26] presented an operational network reconfiguration strategy in the event of high winds, to maximize network resilience and minimize the number of line switches simultaneously. Sometimes, islanding or not islanding after disruptive events are treated differently. Agrawal et al. [27] developed a self-healing algorithm to restore the maximum priority loads by reconfiguring network, without intentional islanding during blackouts. Guimaraes et al. [28] proposed a three-stage algorithm for the dynamic reconfiguration of distribution networks with islanding. The three stages of the algorithm included calculating the network reconfiguration solutions in each hour, reducing the number of configurations, and generating the optimal sequence of topologies. Li et al. [29] developed a concept of a fully decentralized multi-agent system to build a restoration service framework for distribution networks. Based on this concept, a network reconfiguration algorithm with intentional islanding was proposed for service restoration. Besides reconfiguration, other corrective actions, such as generator re-dispatch, control of distributed energy storage systems (ESSs), and on-load tap changers, can also be considered as supplementary strategies to enhance power system resilience. Liberati et al. [30] proposed a control system, which optimized grid operations through network reconfiguration, control of distributed energy storage systems and on-load tap changers. Sekhavatmanesh and Cherkaoui [31] developed an analytical and global optimization model to find the most efficient restoration plan with the goal of minimizing the number of de-energized nodes and minimizing the number of corrective actions as well. The considered corrective actions included network reconfiguration, the tap setting modification of voltage regulation devices, the nodal load-rejection, and the active/reactive power dispatch of distribution generators. Zhang et al. [32] introduced two-stage stochastic models to deal with the uncertainty in generation and demand during the recovery process. Switching transmission lines and generator re-dispatch strategies were used to maximize load shed recovery in the bulk transmission network. Nazemi and Dehghanian [33] introduced a framework for modeling seismic and vulnerability of electric power systems. The generation re-dispatch strategy and corrective network topology control were considered to maximize the load outage recovery after earthquakes. Gholizadeh et al. [34] proposed a model to obtain the optimal allocation of sectionalizing switches and fuses while the economical loss of both DG units and electricity customers were taken into consideration. The results showed that the DG units and their economical loss could significantly influence the placement of switch and fuse placement when tie switches did not exist in the network.

Some studies [35] treat the RN as an independent system in restoration planning. For short-term restoration, reconfiguring network topology, controlling traffic lights and traffic demands management are frequently adopted. For example, Wang and Wang [36] developed an integrated reconfiguration strategy that considered the reconfiguration along both the supply and demand sides of the transportation system. The traffic demand was reconfigured using a heterogeneous fleet of vehicles and the network topology was reconfigured through a heterogeneous contraflow control. Later on, they further refined the framework [37] for resilience analysis in consideration of measurement and improvement. Two strategies were used to maximize the system resilience. The first one used integrated reconfiguration of both traffic supply and demand to reduce traffic demand through combining different traffic modes. The second one employed a contraflow strategy to increase traffic capacity. Chiou [38] proposed a period-dependent traffic responsive signal control model to enhance resilience of urban RNs. Koutsoukos et al. [39] developed a modeling and simulation integration platform for experimentation and evaluation of resilient transportation systems. Resilient traffic signal control in the presence of denial-of-service attacks was studied

in the case studies. Regarding the long-term recovery period, scheduling repair crew, allocating resources and determining restoration priority of components [40] in the RNs are the common strategies. Wu et al. [41] proposed a methodology to assess the resilience of transportation networks and a restoration priority measure was developed to support post-earthquake restoration of damaged bridges. Zhao and Zhang [42] proposed a bi-objective bi-level optimization framework to determine an optimal transportation network restoration plan. The lower-level problem considered elastic user equilibrium to model the imbalance between demand and supply. The upper-level problem, formulated as bi-objective mathematical programming, determined the optimal resource allocation for roadway restoration.

With the increasingly coupled RNs and PNs, considering the two networks as a whole has become a need [43, 44]. Currently, only a few studies have investigated how to restore a coupled traffic-power network after disruptions in an integrated way. Among these studies, considered restoration strategies include optimally routing and scheduling mobile energy storage systems (MESSs)/mobile energy sources [45, 46, 47, 48], coordinating with repair crews [46, 47, 48] and switching lines [46, 47]. Most above-mentioned studies assume that only the PNs are damaged by the disruption, whereas the RNs are not influenced and the time to transport the restoration resources is the same as normal situation. However, the RNs may also be damaged during the disruption, thus, the efficiency of the RNs may decrease. Only several works considered that the disruption caused influences on both networks. Wang et al. [49] considered the PNs and urban RNs coupled through traffic lights and mobile emergency resources (i.e., mobile emergency generators, MESSs, electric buses and repair crews) for PNs. The availability of mobile emergency resources for load restoration in PNs is related to their dispatch in the RNs, and the effect of PN-enabled traffic lights on traffic flow is also modeled. They developed a service restoration method to maximize the efficiency of both PNs restoration and RNs. Yao et al. [50] proposed a rolling integrated service restoration strategy to minimize the total system cost by coordinating the scheduling of MESS fleets, resource dispatching of microgrids and network reconfiguration of PNs. The integrated strategy considered damage and repair to both the roads in RNs and the branches in PNs. Li et al. [51] presented an optimization model for joint post-disaster PN restoration, considering coordinated dispatching with electric buses of vehicle-to-grid (V2G) storage capability. Idle buses placed at designated areas can feed power back to the grid via charging equipment in case of need. The schedule of the remaining buses should meet the passenger transport demand. Belle et al. [52] proposed a model to analyze the vulnerability of coupled railway and PNs where the power network acted as an interface. They showed that failures in the power network could cause a negative impact on the railway network.

Above-mentioned studies considered different interfaces between PNs and RNs. How to properly model the interfaces of the two networks is another key issue in investigating the optimal service restoration of traffic-power networks. This paper considers that the RNs and PNs are coupled through grid-enabled electric vehicles (EVs) and fast-charging stations (FCSs), which are increasingly being deployed around the world [53]. Meanwhile, the risk of power outages in FCSs due to natural disaster have raised serious concerns [54, 55]. This aspect has not been paid much attention in the current literature.

In this paper, we focus on the emergency response problem for the coupled traffic-power networks through grid-enabled EVs and FCSs. The target of this problem is using the available resources to quickly recover partial system service when the two networks are both damaged in a disruptive event. The intensively investigated long-term restoration problem is out of the scope of the present paper. For the emergency response strategies, the links reversing is considered, because it can be easily taken as an operational response in most cases and also provide flexibility

to quickly restore part of the disrupted transport services. Other strategies are not considered since, for example, traffic light controlling is not applicable to the electrified highway networks; Traffic demand management is usually used for evacuation planning and, thus, is not appropriate in our problems. Switching transmission lines are considered as emergency response strategy for the PNs, since it almost is the most urgent first response. In RNs, vehicles may need to detour and the RNs' performance, evaluated in terms of the satisfied traffic demand on a certain period of time, therefore, may decrease. Due to the detoured vehicles, both the number of EVs and the amount of charging demand for individual EV may increase in FCSs. Such charging demand may become a burden for post-disruption PNs and the PNs may need to shed partial EV charging load to protect the PNs from a total blackout. Consequently, the unavailability of the service in FCSs can further influence the charging demand patterns and decrease the performance of the RNs. However, in the current literature, there is a lack of models that are able to describe the above-mentioned interactions within the two networks.

To fill the research gaps described before, this paper proposes a mixed integer program model to minimize the performance loss of the coupled traffic-power systems upon the occurrence of disruptive events. In our paper, the system performance loss is measured by the unsatisfied travel demand and electricity demand. The unsatisfied/satisfied demand is a commonly used performance indicator to be optimized for both the power and transportation systems in the resilience-related literature. For example, Ref. [56] maximized the weighted sum of restored loads, Ref. [57] minimized the total amount of lost power during the restoration process and Ref. [13] used the energy not supplied as the indicator to estimate the system resilience. For the transportation systems, minimizing the functionality losses of RNs [14], minimizing unmet demand [42], maximizing network throughput [58] can be frequently found in the literature. For the interdependent systems, they are assumed to be integrally operated by one decision-making agent, therefore, minimizing the total system performance loss (i.e., total unsatisfied demand) [59, 60] is proposed naturally. In this work, we firstly formulate the emergency response problem based on network topology reconfiguration for the independent electrified RNs and PNs, respectively. Then, the emergency response problem for the coupled traffic-power system is proposed from a centralized decision-making perspective. Specifically, an integrated traffic-power systems model is developed to describe the dynamic interaction between RNs and PNs, through EVs and spatiotemporal distributed charging demand.

The main contributions of this paper are summarized as follows:

1. Most of the existing work studies PNs and RNs separately, or assumes that one single system is damaged by a disruption. This work treats the PNs and RNs as a whole and assumes both of them are partially damaged, where the degraded services influence each other.
2. To the best of our knowledge, this is the first work that investigates the emergency response problem for the traffic-power systems coupled through grid-enabled EVs and FCSs.
3. A new integrated model is presented to explicitly model the interaction between PNs and RNs, where the system optimal dynamic traffic assignment problem and the DC optimal power flow problem are embedded, and the physical constraints from both networks are considered.
4. The strategies of link directions reversing in RNs and line switching in PNs are mathematically formulated and originally modeled to mitigate the system performance loss in an interdependent traffic-power system environment, and in independent RN and PN environments, respectively.

The remainder of the paper is structured as follows. Section 2 formulates the reconfiguration problems in independent RN and PN, as well as in the interdependent traffic-power system. Section 3 illustrates a case study to show the application of the proposed models and compares the solutions under different response resource levels, EV penetration levels and decision-making environments. Finally, Section 4 provides concluding remarks and future research directions.

2. Infrastructures models and reconfiguration problem formulation

In this section, models for the reconfiguration of independent RNs, independent PNs and interdependent traffic-power systems are formulated.

2.1. Reconfiguring electrified road networks

In this subsection, we present an electrified traffic system model considering the critical characteristics of EVs and FCSs. The model is based on the link transmission model (LTM) appraoch. The emergency response problem for the electrified RNs with reconfiguration techniques after disruption problem is, then, formulated based on the electrified traffic model presented. The main flowchart of the proposed methodology is shown in Figure 1.

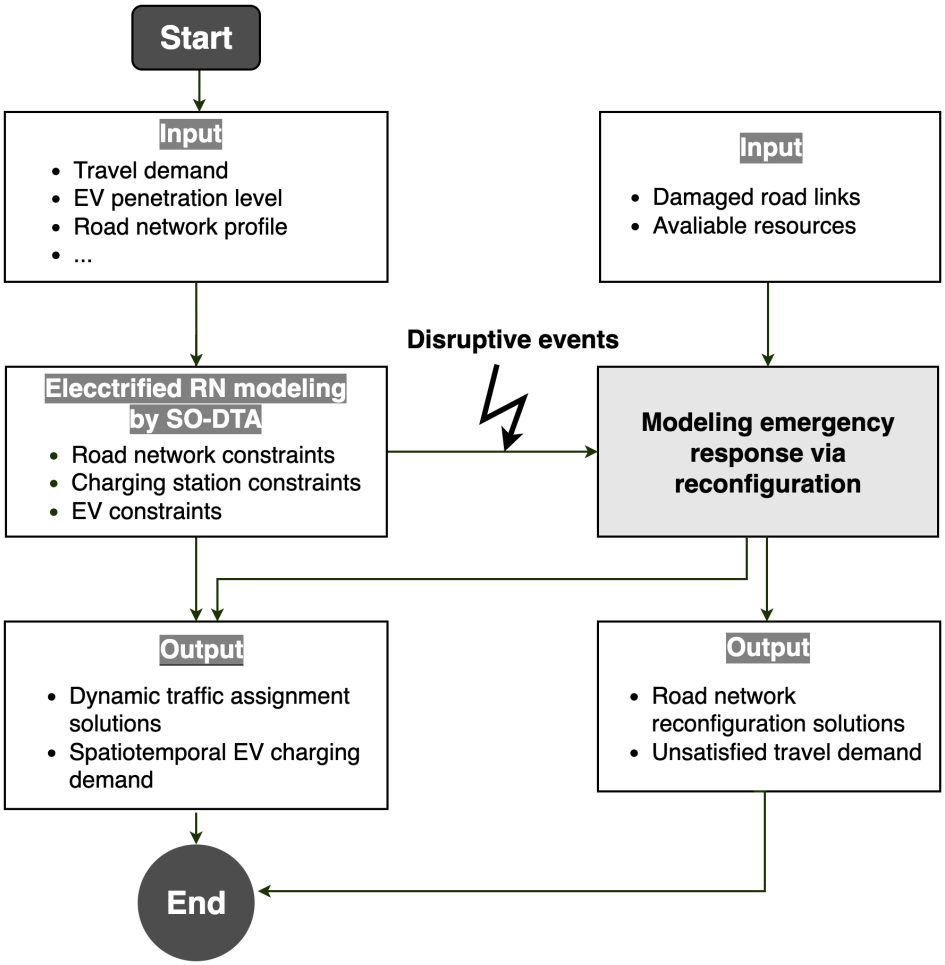

Figure 1: The main flowchart of modeling electrified road networks and its emergency response problem.

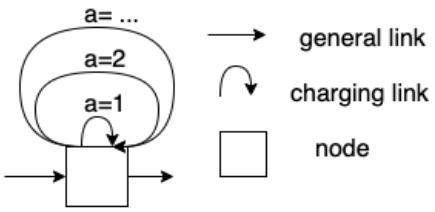

Figure 2: Link representation of different types of charges within a charging station.

2.1.1. Modeling electrified road networks

In this model, we assume that the electricity consumed by an EV is linearly related to the distance traveled. The electricity amount charged by an EV is linearly related to the charging time. All EV batteries have the same energy consumption efficiency, similar to Ref. [61].

A RN with multiple sources (origins) and sinks (destinations) is here denoted as $G(\mathcal{N}, \mathcal{A})$, where $\mathcal{N}$ and $\mathcal{A}$ are the sets of nodes and links, respectively. Links in the RN are classified into four types: source $\mathcal{A}_R$, sink $\mathcal{A}_S$, general $\mathcal{A}_G$ and charging $\mathcal{A}_C$ links. Dummy charging links $\mathcal{A}_C$ are originally defined to describe the FCS in the physical RN. A FCS is modeled by one or several charging links, represented by arcs having the same origin and destination, as shown in Figure 2. Chargers with different charging speeds are represented by different charging links.

Nodes are classified into two types: source-sink $\mathcal{N}_{SR}$ and general $\mathcal{N}_G$ nodes. Within the RN, each source-sink node connects only one source and one sink link. All charging, source and sink links are dummy with lengths 0 so that no unnecessary travel time is counted on these dummy links. All source and sink links are with infinite outflow, inflow and storage capacities so that they will never become the bottlenecks of the traffic flow in the modeled RN. For the system optimal dynamic traffic assignment (SO-DTA) problem, the outflow capacity of all sink links are assumed to be 0, similar to Refs. [62, 63, 64]. It means that all vehicles are collected upon their arrival. The time horizon H is discretized into a finite set of periods $\mathcal{T} = \{t = 1, 2, \cdots, T\}$. T is calculated according to $T = H/\delta$, where δ is the period length. The period length should be equal to or smaller than the smallest link travel time so that vehicles take at least one time unit to traverse a link [65].

A triangular fundamental diagram is defined in LTM, as an approximation of the macroscopic properties of roads [65]. The diagram is defined by three parameters: a jam density (k_{jam}), a maximum flow (q_{max}) and a fixed-free flow speed (v_f). The backward shock-wave speed w can be obtained by $w = q_{max} \cdot v_f/(q_{max} - k_{jam} \cdot v_f)$.

Given a certain class of EV denoted as c, its battery capacity is B_c kWh and the energy consumption efficiency is η kWh/mile, then, the mileage of this class EV is $L_c^{max} = B_c/\eta$ miles. We discretize its mileage into integer energy levels (ELs). When this EV has full battery, it has the maximum EL $E_c = L_c^{max}/(\delta \cdot v_f)$. Once this EV traveled $\delta \cdot v_f$ miles, its ELs decrease one unit EL, i.e., 1 unit EL $= \delta \cdot v_f$ miles. We assume that there are C EV classes represented as $\mathcal{C} = \{\mathcal{E}_1, \mathcal{E}_2, \cdots, \mathcal{E}_C\}$. Each element $\mathcal{E}_c$ in set $\mathcal{C}$ is a set, which contains the energy levels that EVs of class c could have, denoted as $\mathcal{E}_c = \{1, 2, \cdots, E_c\}$.

In the LTM, the traffic flow dynamic evolution is obtained by calculating the cumulative number of vehicles at entry and exit of each link, in each period of time t.

Newell's simplified theory [66, 67] is used in LTM to calculate sending $S_a(t)$ and receiving $R_a(t)$

capacities of link a:

$$S_a(t) = \min\{U_a(t-\nu_a) - V_a(t-1), f_a^O(t)\} \tag{1a}$$

$$R_a(t) = \min\{V_a(t-\beta_a) + L_a \cdot k_{jam} - U_a(t-1), f_a^I(t)\} \tag{1b}$$

where $U_a(t)/V_a(t)$ denotes the cumulative number of vehicles that enter/leave link a by the end of period t. $f_a^I(t)$ and $f_a^O(t)$ are the inflow capacity at the entering point and outflow capacity at the leaving point of link a during period t, respectively. They can be obtained by computing $\delta \cdot q_{max}$ at the corresponding location and period. L_a is the length of link a. ν_a is the free-flow travel time on link a and β_a is the travel time required by the backward shock wave from the exit to the entry of link a. They can be obtained by $\nu_a = L_a/(\delta \cdot v_f)$ and $\beta_a = L_a/(\delta \cdot w)$, respectively.

The inflow and outflow of link a during interval t are constrained by its corresponding sending and receiving capacities:

$$U_a(t) - U_a(t-1) \leq R_a(t), \forall a \in \mathcal{A}\backslash\{\mathcal{A}_C\}, \forall t \tag{2a}$$

$$V_a(t) - V_a(t-1) \leq S_a(t), \forall a \in \mathcal{A}\backslash\{\mathcal{A}_C\}, \forall t \tag{2b}$$

Substituting Eqs. (1) and (1b) into the system of inequality (2), we obtain the following system of linear LTM-based flow constraints:

$$V_a(t) \leq U_a(t-\nu_a), \forall a \in \mathcal{A}\backslash\{\mathcal{A}_C\}, \forall t \tag{3}$$

$$V_a(t) - V_a(t-1) \leq f_a^O(t), \forall a \in \mathcal{A}\backslash\{\mathcal{A}_C\}, \forall t \tag{4}$$

$$U_a(t) - U_a(t-1) \leq f_a^I(t), \forall a \in \mathcal{A}\backslash\{\mathcal{A}_C\}, \forall t \tag{5}$$

$$U_a(t) - V_a(t-\beta_a) \leq L_a k_{jam}, \forall a \in \mathcal{A}\backslash\{\mathcal{A}_C\}, \forall t \tag{6}$$

In the proposed LTM-based model, both EVs and conventional vehicles are considered as follows :

$$U_a(t) = \sum_{s\in\mathcal{N}_S} UG_a^s(t) + \sum_{s\in\mathcal{N}_S}\sum_{c\in\mathcal{C}}\sum_{e\in\mathcal{E}_c} UE_{a,c}^{s,e}, \forall a \in \mathcal{A}\backslash\{\mathcal{A}_C\}, \forall t \tag{7a}$$

$$V_a(t) = \sum_{s\in\mathcal{N}_S} VG_a^s(t) + \sum_{s\in\mathcal{N}_S}\sum_{c\in\mathcal{C}}\sum_{e\in\mathcal{E}_c} VE_{a,c}^{s,e}, \forall a \in \mathcal{A}\backslash\{\mathcal{A}_C\}, \forall t \tag{7b}$$

where $UE_{a,c}^{s,e}(t)/VE_{a,c}^{s,e}(t)$ denotes the cumulative number of EVs that belong to type c with EL e, that enter/leave link a to destination s by the end of period t; $UG_a^s(t)/VG_a^s(t)$ denotes the cumulative number of GVs that enter/leave link a to destination s by the end of interval t.

Substituting Eq. (7) into the inequalities in Eqs. (3) - (6), we can have the following constraints for the mixed traffic of EVs and GVs:

$$\sum_{s\in\mathcal{N}_S}[VG_a^s(t) - VG_a^s(t-1)] + \sum_{s\in\mathcal{N}_S}\sum_{c\in\mathcal{C}}\sum_{e\in\mathcal{E}_c}[VE_{a,c}^{s,e}(t) - VE_{a,c}^{s,e}(t-1)] \leq f_a^O(t), \forall a \in \mathcal{A}\backslash\{\mathcal{A}_C\}, \forall t, s \tag{8}$$

$$\sum_{s\in\mathcal{N}_S}[UG_a^s(t) - UG_a^s(t-1)] + \sum_{s\in\mathcal{N}_S}\sum_{c\in\mathcal{C}}\sum_{e\in\mathcal{E}_c}[UE_a^s(t) - UE_a^s(t-1)] \leq f_a^I(t), \forall a \in \mathcal{A}\backslash\{\mathcal{A}_C\}, \forall t, s \tag{9}$$

$$\sum_{s\in\mathcal{N}_S}\sum_{c\in\mathcal{C}}\sum_{e\in\mathcal{E}_c}[UE^{s,e}_{a,c}(t)-VE^{s,e}_{a,c}(t-\beta_a)]+\sum_{s\in\mathcal{N}_S}[UG^s_a(t)-VG^s_a(t-\beta_a)] \le L_a k_{jam}, \forall a\in\mathcal{A}\backslash\{\mathcal{A}_C\}, \forall t, s \tag{10}$$

For GVs, the cumulative outflow disaggregated by destinations should also be constrained by the boundary condition at the inflow. Hence, we have

$$\sum_{s\in\mathcal{N}_S} VG^s_a(t) \le \sum_{s\in\mathcal{N}_S} UG^s_a(t-\nu_a), \forall a\in\mathcal{A}\backslash\{\mathcal{A}_C\}, \forall t \tag{11}$$

For EVs, the disaggregated cumulative outflow should also be constrained by the battery condition at the inflow. Hence, we have

$$VE^{s,e}_{a,c}(t) \le UE^{s,e+\rho_a}_{a,c}(t-\nu_a), \forall a\in\mathcal{A}\backslash\{\mathcal{A}_C\}, e\in\mathcal{E}_c\cap\{e\le E_c-\rho_a\}, \forall s,c,t \tag{12a}$$

$$VE^{s,e}_{a,c}(t) = 0, \forall a\in\mathcal{A}\backslash\{\mathcal{A}_C\}, e\in\mathcal{E}_c\cap\{e> E_c-\rho_a\}, \forall s,c,t \tag{12b}$$

where, ρ_a is the ELs required to traverse link a and it is calculated by $\rho_a = L_a/(\delta\cdot v_f)$. Eq. (12a) guarantees that outflow should be less than or equal to the inflow. It also guarantees that the outflow ELs are updated from the inflow after the EVs traversed the corresponding links. Eq. (12b) ensures that all EV ELs should be less than their maximum ELs.

The traffic demand is satisfied by letting the cumulative inflows of source links equal the cumulative demands:

$$UG^s_a(t) = DG^s_a(t), \forall a\in\mathcal{A}_R, \forall s,t \tag{13a}$$

$$UE^{s,e}_{a,c}(t) = DE^{s,e}_{a,c}(t), \forall a\in\mathcal{A}_R, e\in\mathcal{E}_c, \forall s,c,t \tag{13b}$$

where $DG^s_a(t)/DE^{s,e}_{a,c}(t)$ represents the cumulative GVs/EVs travel demand between the entry of origin link a and destination s at the end of period t.

The inflow and outflow of a general node should be restricted by the following flow conservation constraints:

$$\sum_{a\in B(i)} VG^s_a(t) = \sum_{b\in A_(i)} UG^s_a(t), \forall i\in\mathcal{N}/\{\mathcal{N}_{SR}\}, \forall s,t \tag{14a}$$

$$\sum_{a\in B(i)} VE^{s,e}_{a,c}(t) = \sum_{b\in A_{(i)}} UE^{s,e}_{a,c}(t), \forall i\in\mathcal{N}/\{\mathcal{N}_{SR}\}, \forall e\in\mathcal{E}_c, \forall s,c,t \tag{14b}$$

where $A(i)/B(i)$ represents the set of links whose tail/head node is i.

For EVs, the current occupancy on charging link a should be limited by the maximum number of chargers on this link:

$$\sum_{s\in\mathcal{N}_S}\sum_{c\in\mathcal{C}}\sum_{e\in\mathcal{E}_c}[UE^{s,e}_{a,c}(t)-VE^{s,e}_{a,c}(t)] \le NC_a(t), \forall a\in\mathcal{A}_C, \forall t \tag{15}$$

where $NC_a(t)$ is the physical number of type a chargers on charging link a during period t.

The following equations are used to update the current occupancy and their ELs on a charging

link:

$$\hat{x}_{a,s}^{s,e}(t) = x_{a,s}^{s,e}(t-1) + [UE_{a,c}^{s,e}(t-1) - UE_{a,c}^{s,e}(t-2)] - [VE_{a,c}^{s,e}(t-1) - VE_{a,c}^{s,e}(t-2)], \forall a \in \mathcal{A}_C, \forall e \in \mathcal{E}_c, \forall s, c, t \tag{16}$$

where $\hat{x}_{a,s}^{s,e}(t)$ and $x_{a,s}^{s,e}(t)$ are the numbers of EVs before and after their ELs have been updated on charging link a.

Based on the obtained occupancies, the following equations are used to model their charging process where ELs of EVs linearly increase with time on charging links:

$$x_{a,c}^{s,E_c}(t) = \sum_{l=0}^{\alpha_a^t} \hat{x}_{a,c}^{s,E_c-l}(t), \forall a \in \mathcal{A}_C, \forall s, c, t \tag{17a}$$

$$x_{a,c}^{s,e}(t) = \hat{x}_{a,c}^{s,e-\alpha_a^t}(t), \quad \forall a \in \mathcal{A}_C, \forall e \in \{\alpha_a^t \le e < E_c\}, \forall s, c, t \tag{17b}$$

$$x_{a,c}^{s,e}(t) = 0, \forall a \in \mathcal{A}_C, \forall e \in \{e < \alpha_a^t\}, \forall s, c, t \tag{17c}$$

where α_a^t represents the average charging speed for charging link a during period t, which translates to how many energy levels can be supplied using type a charger during a period δ. Assuming the charging power of charging link a is p_a^{ev}, then, α_a^t can be calculated by $\frac{p_a^{ev} \cdot \delta}{\eta \cdot \delta \cdot v_f} = \frac{p_a^{ev}}{\eta \cdot v_f}$. Eqs. (17a) and (17c) constraint the upper and lower boundaries of the updated ELs. Eq. (17b) describes the process of linear increase in ELs.

Additionally, the outflow disaggregated by each EL on charging link a should be less than its occupancy, as formulated in Eq. (18):

$$VE_{a,c}^{s,e}(t) - VE_{a,c}^{s,e}(t-1) \le x_{a,c}^{s,e}(t), \forall a \in \mathcal{A}_C, \forall e \in \mathcal{E}_c, \forall s, c, t \tag{18}$$

The occupancies on charging links are nonnegative, which is formulated as follows:

$$x_{a,c}^{s,e}(t) \ge 0, \ \hat{x}_{a,c}^{s,e}(t) \ge 0, \forall a \in \mathcal{A}_C, \forall e \in \mathcal{E}_c, \forall s, c, t, \tag{19}$$

The cumulative flows should be nonnegative and nondecreasing:

$$VG_a^s(t) - VG_a^s(t-1) \ge 0, \forall a \in \mathcal{A}, \forall s, t \tag{20a}$$

$$VE_{a,c}^{s,e}(t) - VE_{a,c}^{s,e}(t-1) \ge 0, \forall a \in \mathcal{A}, \forall e \in \mathcal{E}_c, \forall s, c, t \tag{20b}$$

$$UG_a^s(t) - UG_a^s(t-1) \ge 0, \forall a \in \mathcal{A}, \forall s, t \tag{21a}$$

$$UE_{a,c}^{s,e}(t) - UE_{a,c}^{s,e}(t-1) \ge 0, \forall a \in \mathcal{A}, \forall e \in \mathcal{E}_c, \forall s, c, t \tag{21b}$$

The following constraints force the initial cumulative flows to be 0:

$$UG_a^s(0) = VG_a^s(0) = 0, \forall a \in \mathcal{A}, \forall s \tag{22a}$$

$$UE_{a,c}^{s,e}(0) = VE_{a,c}^{s,e}(0) = 0, \forall a \in \mathcal{A}, \forall e \in \mathcal{E}_c, \forall s, c \tag{22b}$$

The objective of electrified RNs model is to minimize the total travel time of all vehicles. The total travel time is calculated by the total presence time of all vehicles on all links during the whole

time horizon and the total charging time of all EVs. Under normal situation, the whole model for the electrified RN is formulated as follows:

$$\begin{aligned}\min \sum_{s\in\mathcal{N}_S}\sum_{t\in\mathcal{T}}\sum_{a\in\mathcal{A}/\{\mathcal{A}_C,\mathcal{A}_S\}} \delta[UG_a^s(t)-VG_a^s(t)] \\ +\sum_{s\in\mathcal{N}_S}\sum_{t\in\mathcal{T}}\sum_{a\in\mathcal{A}/\mathcal{A}_S}\sum_{c\in\mathcal{C}}\sum_{e\in\mathcal{E}_c}\delta[UE_{a,c}^{s,e}(t)-VE_{a,c}^{s,e}(t)]\end{aligned} \tag{23}$$

subject to:

$$\text{Eqs. (7)} - \text{(22)} \tag{24}$$

2.1.2. Modeling reconfiguration strategy in electrified road networks

To mitigate the impacts after disruptions, we consider the strategy of contraflow to reconfigure the topology of the highway networks. Contraflow can be easily implemented by reversing the direction of lanes of highway networks. Fig. 3 shows how the contraflow assists increasing the throughput of the network after disruptions. Assuming that there are 20 vehicles per minute starting from node O to D and 10 vehicles per minute from node D to O. The number along each link represents the time required to traverse the link at a free-flow speed. Fig. 3(a) shows that there are 30 and 60 vehicles arriving at nodes O and D, respectively, after 6 minutes, when each link works normally. If the link from node O to D fails, the arrivals on node D decrease to 40 vehicles, as shown in Fig. 3(b). However, if we reverse the direction of the link a_1, the total number of arrivals can be increased from 70 to 80 vehicles after the disruption, as shown in Fig. 3(c). This example shows that reconfiguring the highway network after disruption could effectively reduce the system performance loss. Another example can be found in Ref. [68], which shows how contraflow strategy increases the network outbound capacity and mitigates congestion.

To model the contraflow strategy, we constrain each link in the highway network to have only one unique opposite link corresponding to it. For example, there are two links a_1 and a_2 from nodes O to D in Fig. 3: their corresponding opposite links are $\hat{a}_1$ and $\hat{a}_2$, respectively. Dually, links a_1 and a_2 are the opposite links of links $\hat{a}_1$ and $\hat{a}_2$. Mathematically, we use variable h_a to denote whether link a is changed to the opposite direction or not. $\hat{a}$ represents the unique opposite link of link a. If the direction of the link is reversed, the outflow capacity, the inflow capacity and the maximum number of vehicles that can be present on that link of direction will be correspondingly reconfigured. Therefore, Eqs. (8) - (10) are reformulated as follows:

$$\begin{aligned}\sum_{s\in\mathcal{N}_S}[VG_a^s(t)-VG_a^s(t-1)]+\sum_{s\in\mathcal{N}_S}\sum_{c\in\mathcal{C}}\sum_{e\in\mathcal{E}_c}[VE_{a,c}^{s,e}(t)-VE_{a,c}^{s,e}(t-1)] \\ \le (1-h_a)\cdot f_a^O(t)+h_{\hat{a}}\cdot f_{\hat{a}}^O(t), \forall a\in\mathcal{A}\backslash\{\mathcal{A}_C\}, \forall t\end{aligned} \tag{25}$$

$$\begin{aligned}\sum_{s\in\mathcal{N}_S}[UG_a^s(t)-UG_a^s(t-1)]+\sum_{s\in\mathcal{N}_S}\sum_{c\in\mathcal{C}}\sum_{e\in\mathcal{E}_c}[UE_a^s(t)-UE_a^s(t-1)] \\ \le (1-h_a)\cdot f_a^I(t)+h_{\hat{a}}\cdot f_{\hat{a}}^I(t), \forall a\in\mathcal{A}\backslash\{\mathcal{A}_C\}, \forall t\end{aligned} \tag{26}$$

$$\begin{aligned}\sum_{s\in\mathcal{N}_S}\sum_{c\in\mathcal{C}}\sum_{e\in\mathcal{E}_c}[UE_{a,c}^{s,e}(t)-VE_{a,c}^{s,e}(t-\beta_a)]+\sum_{s\in\mathcal{N}_S}[UG_a^s(t)-VG_a^s(t-\beta_a)] \\ \le (1-h_a)L_a k_{jam}+h_{\hat{a}}L_{\hat{a}}k_{jam}, \forall a\in\mathcal{A}\backslash\{\mathcal{A}_C\}, \forall t\end{aligned} \tag{27}$$

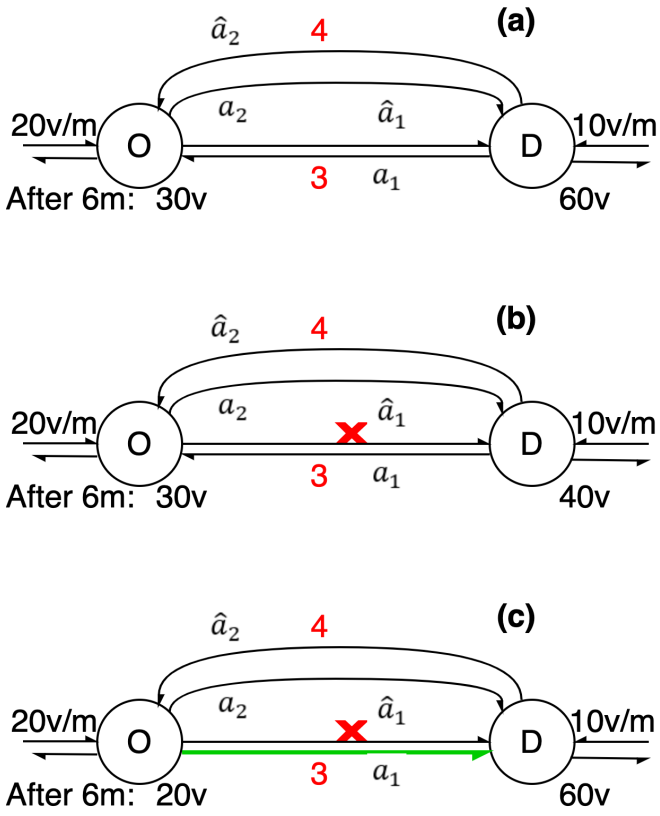

Figure 3: Contraflow illustration: (a) Normal condition (b) After disrutption (c) After reconfiguration

Eq. (25) states that the outflow on link a are constrained by the status of links a and $\hat{a}$. If $h_a = 0$ and $h_{\hat{a}} = 0$, no link is reversed and the outflow capacity on the direction of original link a is unchanged, i.e., the outflow capacity of link a; if $h_a = 1$ and $h_{\hat{a}} = 1$, both links are reversed and the outflow capacity is modified to the outflow capacity of link $\hat{a}$; if $h_a = 1$ and $h_{\hat{a}} = 0$, the direction of link a is reversed and the outflow capacity becomes 0; if $h_a = 0$ and $h_{\hat{a}} = 1$, the direction of the opposite link $\hat{a}$ is reversed and the outflow capacity increase to the sum of outflow capacities of links a and $\hat{a}$. Similarly, we can have Eqs. (26) and (27) to constrain the inflow and maximum occupancies on the direction of original link a after reconfiguration:

$$h_a, h_{\hat{a}} \in \{0,\ 1\}, \forall a, \hat{a} \in \mathcal{A} \backslash \{\mathcal{A}_C\} \tag{28}$$

$$\sum_{a \in \mathcal{A} \backslash \{\mathcal{A}_C\}} h_a \leq N_h \tag{29}$$

Eq. (28) guarantees that h_a and $h_{\hat{a}}$ are binary variables. Eq. (29) constrains the total number of links that can be reversed. This constraint reflects the limited resources that can be used in emergency response.

The emergency response problem for electrified RNs with contraflow options is formulated as follows:

$$\min \sum_{s \in \mathcal{N}_S} \sum_{t \in \mathcal{T}} \sum_{a \in \mathcal{A}_S} [DG_a^s(t) - UG_a^s(t) + \sum_{c \in \mathcal{C}} \sum_{e \in \mathcal{E}_c} (DE_{a,c}^{s,e}(t) - UE_{a,c}^{s,e}(t))] \cdot \phi \tag{30}$$

subject to:

$$\text{Eqs. (11)} - \text{(29)} \tag{31}$$

where ϕ denotes the time value. The objective of the transportation operator is to minimize the system performance loss cost, measured by the unsatisfied traffic demand, after disruptions within a certain period. More specifically, it is calculated by the cumulative difference between the target demand (i.e., $DG_a^s(t)$ and $DE_{a,c}^{s,e}(t)$) and the number of vehicles arrived at their destinations (i.e., $UG_a^s(t)$ and $UE_{a,c}^{s,e}(t)$, $a \in \mathcal{N}_S$). In Eq. (30), the first term is the cumulative unsatisfied GVs travel demand and the second term is the cumulative unsatisfied EVs travel demand.

2.2. Reconfiguring power networks

In this subsection, the classic DC optimal power flow (OPF) model [69] is used to model the transmission network operation. Based on this model, the emergency response problem for the PN using switch options is formulated. The main flowchart of modeling power networks and its emergency response problem is shown in Figure 4.

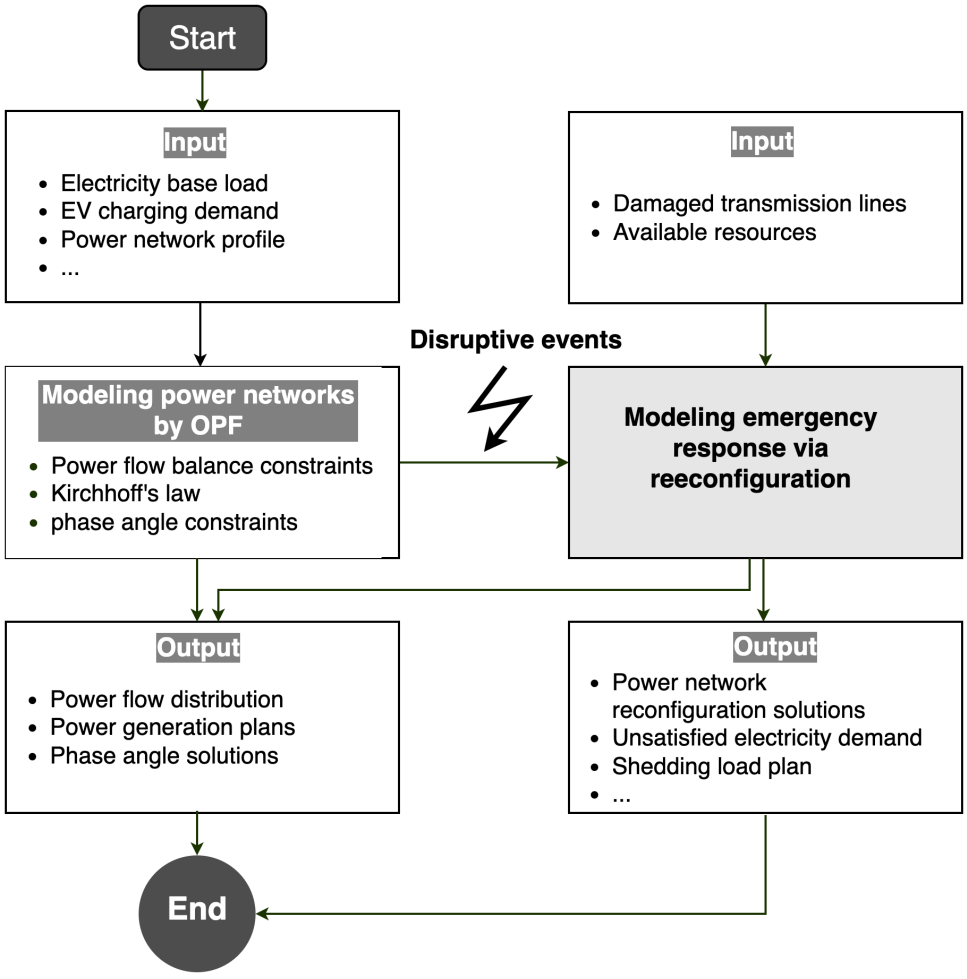

Figure 4: The main flowchart of modeling power networks and its emergency response.

We consider a PN $\mathcal{G}_P(\mathcal{P}_N, \mathcal{P}_L)$, where $\mathcal{P}_N$ and $\mathcal{P}_L$ represent the sets of buses and branches, respectively. $\widetilde{\mathcal{P}}_L$ represents the set of damaged transmission lines after a disruption, $\widetilde{\mathcal{P}}_L \subset \mathcal{P}_L$. $\Gamma^-(j)$ and $\Gamma^+(j)$ denote the sets of predecessors and successors of bus j, respectively.

After the disruption, the objective of the independent system operator is to minimize the cost of unsatisfied load demand, which is formulated as follows:

$$\min P_P = \sum_j \sum_t [c_j^b \cdot LS_{j,t}^b + c_j^{dc} \cdot LS_{j,t}^{dc} \cdot p_j^{dc}(t)] \cdot w_j \tag{32}$$

where c_j^b and c_j^{dc} are the costs of shedding base load and EV charging load, respectively; w_j, with, $\sum_j w_j = 1$, denotes the priority weight of load bus j, which can be heuristically determined, e.g., by considering the nature and importance of the load at each bus; $LS_{j,t}^b$ is a continuous variable representing the amount of unsatisfied base demand at bus j in period t; $LS_{j,t}^{dc}$ is a binary variable denoting where the charging demand $p_j^{dc}(t)$ at bus j in period t is shedded or not.

The power flows in the PN are subjected to the following constraints:

$$p_{j,t}^g + \sum_{i \in \Gamma^-(j)} P_{i,j,t} - \sum_{k \in \Gamma^+(j)} P_{j,k,t} = p_{j,t}^b - LS_{j,t}^b + (1 - LS_{j,t}^{dc}) \cdot p_j^{dc}(t), \forall j \in \mathcal{P}_N, \forall t \tag{33}$$

$$-\bar{P}_{i,j} \cdot u_{i,j} \leq P_{i,j,t} \leq \bar{P}_{i,j} \cdot u_{i,j}, \forall (i,j) \in \mathcal{P}_L \backslash \{\widetilde{\mathcal{P}}_L\}, \forall t \tag{34}$$

$$P_{i,j,t} = 0, \forall (i,j) \in \{\widetilde{\mathcal{P}}_L\}, \forall t \tag{35}$$

$$B_{i,j} \cdot (\theta_{i,t} - \theta_{j,t}) - P_{i,j,t} + (1 - u_{i,j}) \cdot M_{i,j} \geq 0, \forall (i,j) \in \mathcal{P}_L \backslash \{\widetilde{\mathcal{P}}_L\}, \forall t \tag{36}$$

$$B_{i,j} \cdot (\theta_{i,t} - \theta_{j,t}) - P_{i,j,t} - (1 - u_{i,j}) \cdot M_{i,j} \leq 0, \forall (i,j) \in \mathcal{P}_L \backslash \{\widetilde{\mathcal{P}}_L\}, \forall t \tag{37}$$

$$-p_j^{ramp} \leq p_{j,t}^g - p_{j,t-1}^g \leq p_j^{ramp}, \forall j \in \mathcal{P}_N, \forall t \in \mathcal{T} \tag{38}$$

$$0 \leq LS_{j,t}^b \leq p_{j,t}^b, \forall j \in \mathcal{P}_N, \forall t \tag{39}$$

$$0 \leq P_{j,t}^g \leq \bar{p}_j^g, \forall j \in \mathcal{P}_N, \forall t \tag{40}$$

$$\sum_{(i,j) \in \mathcal{P}_L} (1 - u_{i,j}) \leq N_u \tag{41}$$

$$u_{i,j} \in \{0,\ 1\}, \forall (i,j) \in \mathcal{P}_L \tag{42}$$

$$LS_{j,t}^{dc} \in \{0, 1\}, \forall j \in \mathcal{P}_N, \forall t \tag{43}$$

Constraint (33) relaxes the power flow balance constraint at each bus by allowing to shed unsatisfied demand. Constraint (34) guarantees that the power flows in the transmission lines do not exceed their capacities if they function. Constraint (35) forces the amount of power flow on the damaged lines to be 0. Constraints (36)-(37) denote Kirchhoff's power flow equations, where power flow are limited by lines' susceptance and the phase angle difference between the two end buses. It is necessary to include the big-M in the equations. In fact, if the constraint is directly written as $B_{i,j} \cdot (\theta_{i,t} - \theta_{j,t}) = P_{i,j,t} \cdot (1 - u_{i,j})$, when the line status is not switched and in service (i.e., $u_{i,j} = 1$), this equation works normally, whereas when the line is switched off (i.e., $u_{i,j} = 0$), the phase angle between the two end buses of this line would be forced to be 0, which is not logical for the power flow in the network. Constraint (38) limits the generator ramp between two successive periods. Constraint (39) gives the lower and upper boundaries of the amount of base load that can be shedded at each bus. Constraint (40) ensures that the flow generated by generators is within their capacity. Constraint (41) limits the number of lines that can be switched. Constraints (42) - (43) state that $u_{i,j}$ and $LS_{j,t}^{dc}$ are binary decision variables.

2.3. Reconfiguring the coupled traffic-power networks

In this subsection, we assume that there is a decision-making agent (e.g., an emergency response authority) that integrally operates and reconfigures the traffic-power networks in a centralized way to minimize the total performance loss of the two systems. The main flowchart of the proposed approach is shown in Figure 5.

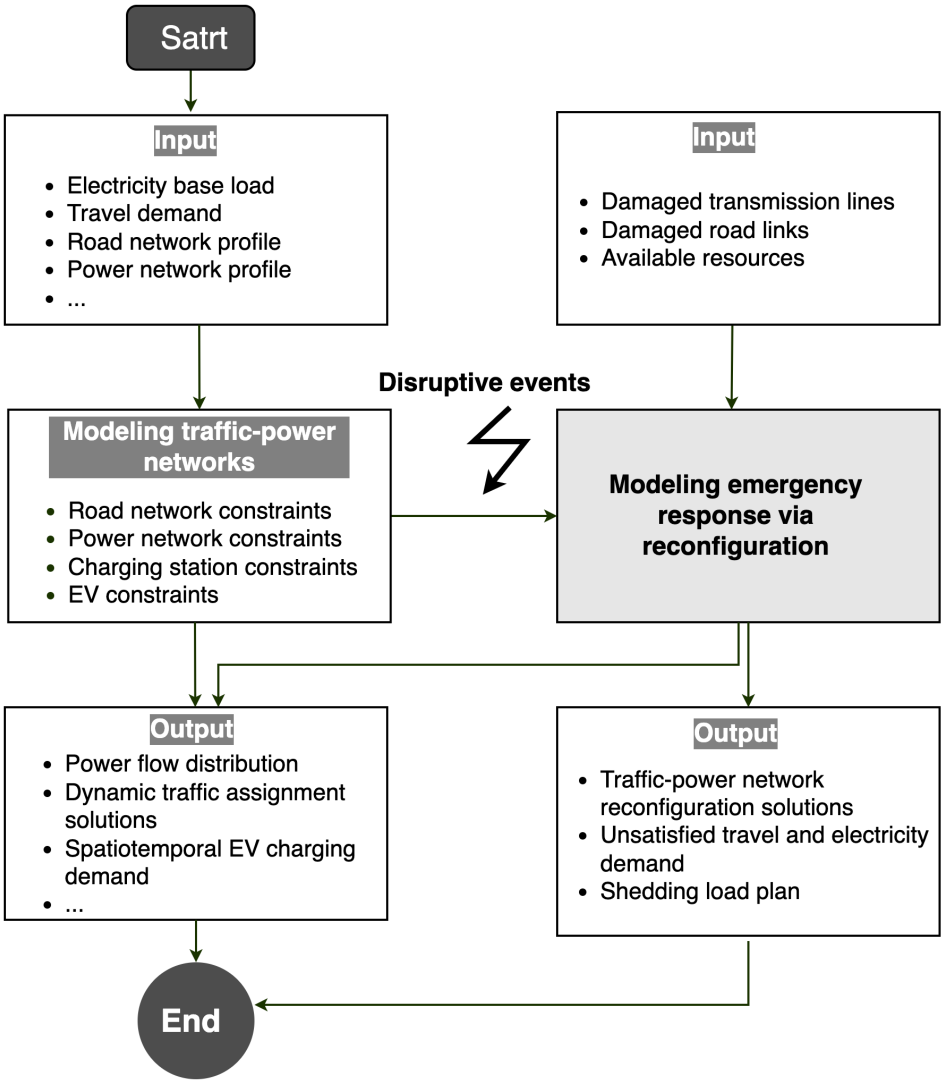

Figure 5: The main flowchart of modeling traffic-power networks and its emergency response problem.

In this situation, the EV charging load $p_j^{dc}(t)$ at each bus becomes a decision variable, which can be calculated by the following equation:

$$p_j^{dc}(t) = \sum_{a \in M(j)} \sum_{s \in \mathcal{N}_S} \sum_{c \in \mathcal{C}} \sum_{e \in \mathcal{E}_c} p_a^{ev} [UE_{a,c}^{s,e}(t) - VE_{a,c}^{s,e}(t)], \forall j \in \mathcal{P}_N, \forall t \tag{44}$$

where $M(j)$ is the mapping from bus set $\mathcal{P}_N$ to charging links set $\mathcal{A}_C$, which specifies the connection between buses in the PN and charging links in the RN.

Since the traffic-power system is integrally operated, the charging locations and times of EVs can be flexibly arranged to contribute to minimizing the objective. Therefore, it is no longer

necessary to have variable $LS_{j,t}^{dc}$ to control whether the EV charging load is shedded or not. Eq. (33) is rewritten as follows:

$$p_{j,t}^{g} + \sum_{i \in \Gamma^{-}(j)} P_{i,j,t} - \sum_{k \in \Gamma^{+}(j)} P_{j,k,t} = p_{j,t}^{b} - LS_{j,t}^{b} + p_{j,t}^{dc}, \forall j \in \mathcal{P}_N, \forall t \tag{45}$$

The whole problem is formulated as follows:

$$\min \sum_{s \in \mathcal{N}_S} \sum_{t \in \mathcal{T}} \sum_{a \in \mathcal{A}_S} [DG_a^s(t) - UG_a^s(t) + \sum_{c \in \mathcal{C}} \sum_{e \in \mathcal{E}_c} (DE_{a,c}^{s,e}(t) - UE_{a,c}^{s,e}(t))] \cdot \phi + \sum_{t \in \mathcal{T}} c_j^b \cdot w_j \cdot LS_{j,t}^b \tag{46}$$

subject to:

$$\text{Eqs. } (11) - (29), (34) - (42) \text{ and } (44) - (45) \tag{47}$$

In each time period, there are expected demand $E(t)$ and unsatisfied demand $\Delta E(t)$ in the system. The following equation is employed to measure the system performance $P(t)$ [1]:

$$P(t) = \frac{E(t) - \Delta E(t)}{E(t)} \tag{48}$$

where $0 \leq \Delta E \leq E$. This equation can be understood as the percentage of demand that can be satisfied in the system in period t.

In the studied traffic-power system, the expected demand includes the all vehicle types traffic demand over all OD pairs and base electricity demand over all buses, which is formulated as follows:

$$E(t) = \sum_{s \in \mathcal{N}_S} \sum_{a \in \mathcal{A}_S} [DG_a^s(t) + \sum_{c \in \mathcal{C}} \sum_{e \in \mathcal{E}_c} DE_{a,c}^{s,e}(t)] \cdot \phi + \sum_{j \in \mathcal{P}_N} c_j^b \cdot p_{j,t}^b \tag{49}$$

where time value ϕ and shedding load cost c_j^b are used, so that the system performance of PNs and RNs have the same physical dimension, and, additivity is allowed.

Substituting Eqs. (46), without summation over time, and (49) into Eq. (48), this letter is rewritten as follows:

$$P(t) = \frac{\sum_{s \in \mathcal{N}_S} \sum_{a \in \mathcal{A}_S} [UG_a^s(t) + \sum_{c \in \mathcal{C}} \sum_{e \in \mathcal{E}_c} UE_{a,c}^{s,e}(t)] \cdot \phi + \sum_{j \in \mathcal{P}_N} [p_{j,t}^b - LS_{j,t}^b] \cdot c_j^b}{\sum_{s \in \mathcal{N}_S} \sum_{a \in \mathcal{A}_S} [DG_a^s(t) + \sum_{c \in \mathcal{C}} \sum_{e \in \mathcal{E}_c} DE_{a,c}^{s,e}(t)] \cdot \phi + \sum_{j \in \mathcal{P}_N} c_j^b \cdot p_{j,t}^b} \tag{50}$$

The proposed emergency response problems for the independent RN (Eqs. 30-31), the independent PN (Eqs. 32-43) and the coupled traffic-power networks (Eqs. 46-47) are mixed integer linear programing problems. Such kind of problems can be efficiently solved by commercial solvers, such as Cplex and Gurobi.

3. Case study

The commonly used IEEE 14-bus system in the literature [70, 71] is adopted as the PN in this study. The original IEEE 14-bus test case is a portion of the American electric power system (in the Midwesten US) [72]. The weight of each bus is assumed to be equal. There are 14 buses and 20 transmission lines, and the detailed data can be found in Ref. [73]. The road network is a partial of the highway network in North Carolina (NC), U.S., and it is shown in Figure 6. Figure 6(a) shows the locations of EV charging stations within this area and the geographic data of the

Table 1: Connections between charging links and buses

Charging link	Bus	$NC_a(t)$
301	2	30
302	3	45
303	4	30
304	5	30
305	6	30
306	7	15
307	8	30
308	9	15

highway network are collected from Google map. This partial highway network is abstracted into an approximated topology network as shown in Figure 6(b). The number along the link is the link ID. There are 9 fast-charging stations in the studied highway network and their connections to the served buses are listed in Table 1. The data used in this study is detailed in Appendix A.

The proposed model is illustrated by solving and analyzing the following hypothetical scenario: it is reported that links 4, 17, 19 in the highway network and lines 2-3, 2-4, 7-8 in the PN are destroyed, and they cannot provide services normally. This scenario is chosen since it causes the most performance loss of the traffic-power system among the randomly generated scenarios, when the number of damaged links in the RN and lines in the PN is 3. In practice, the disruption scenarios are the input data of the proposed models. They can be detected by various manner (e.g., drones and online monitoring systems) after disruptive events. After the system status is collected, the proposed models can be utilized to assist the emergency response department solve the problem: how to reconfigure and operate both the traffic and power systems, so that their performance loss caused by the disruption can be minimized. In this example, the peak hours (i.e., 17:00-18:59) are studied to consider the worst-case scenarios.

All of the numerical experiments have been run on a computer with an Intel Core i7-8700 3.2-GHz CPU with 32 GB of RAM. All of the problems have been solved by the commercial software IBM ILOG CPLEX (version 20.1.0.0).

3.1. The impact of the different response resource level

In this subsection, five different resource levels are investigated: $N_h = N_u = 0,\ 1,\ 2,\ 3,\ 4,\ 5$. Figure 7 shows the system performance evolution over the considered time horizon under different resource levels. Time step = 0 indicates the point in time of implementation of the reconfiguration. The performance level denotes the percentage of the total demand that is satisfied. It can be seen that the system performance levels are different under different resource levels. In practice, the system performance increases with the resource levels, as expected. Note that when the PN topology is reconfigured, the effect (i.e., the shedded load) is seen almost immediately. On the contrary, the effect of reconfiguring an highway network is seen later, due to the time delay required by the vehicles to complete their travel from origin to destination. If the response resource level increases from 0 to 2, the system performance is largely increased from 76.58% to 86.26%. After that, the marginal economic benefit of additional response resources reduces as the number of links reversing and lines switching rises. This can also be seen in Figure 8. When the resource level is 2, the nominal costs of both the RN and the PN reduce largely. This also shows the effectiveness of reconfiguring network topology during the restoration period. Table 2 shows the reconfiguration solutions of links in the RN and of lines in the PN. The third through the fifth columns represent

Table 2: Solutions under different resource levels

Resource levels	$h_a = 1$	$u_{i,j} = 0$	Vehicles	GVs	EVs	Charging demand (MW)
0			19091	17336	1755	182.8
1	117	4-7	22142	20322	1820	148.8
2	104,117	4-9,7-9	21573	19512	2061	165.68
3	5,104,117	4-7,4-9,6-13	21987	19656	2331	207.68
4	5,26,114,117	4-7,4-9,1-2,9-14	22005	19669	2336	222.88
5	5,25,26,114,117	4-7,4-9,1-2,6-12,13-14	21999.5	19656	2343.5	201.28

the number of GVs and EVs arrived at destination at the end of the studied horizon. The last column represents the total charging demand during the studied horizon. The third column in Table 2 shows that the optimal set of the switched lines for low resource level scenarios is not necessarily a subset of the switched lines for high resource level scenarios. For instance, line 4-7 is switched off when resource level is 1, whereas lines 4-9 and 7-9 are switched off when resource level increases to 2. However, this is not applied to the RN in this example. There could be two reasons related to the traffic demand distribution: 1) the used gravity model generates high traffic demand between two cities whose distance is short and population is large. This may cause high traffic volume on some two-way road sections; 2) to model the directional differences of traffic volumes, the direction of traffic demand between two cities is randomly selected. This could make the bidirectional high traffic volumes become one-way high traffic volumes on some road sections. Therefore, once the links with high traffic volumes are damaged (e.g., links 17 and 19), they may always have priority of restoration so that the system loss can be minimized. Moreover, when there are large volume differences between two opposite links, the link capacity can be greatly improved by reversing the link with less volumes (e.g., links 5 and 26). In this sense, less nominal cost of system performance loss and higher resource level do not mean that more vehicles can arrive at the destinations. For example, Figure 8 shows that the nominal loss cost when resource level is 2, is less than that when resource level is 1. However, Table 2 shows that there are also less arrivals when the resource level is 2 than when the resource level is 1. It is because the vehicles arrive at their destinations earlier when the resource level is 2 than when the resource level is 1. In other words, there is a trade-off between the number of arrivals and their travel time for RNs.

3.2. Different EV penetration levels and decision environments

Without loss of generality, the maximum number of lines that can be switched in the PN and of links that can be reversed in the RN are set to be 3 (i.e., $N_u = 3$ and $N_h = 3$). When the RN and PN independently optimize their restoration plans, we assume that the RN operators share their temporal and spatial charging demand with the PN operators at the beginning of the restoration horizon and they no longer change their plans afterwards. This situation can be regarded as the unmanaged charging demand scenarios from the PN operator perspective. In this case, the PN operators have to satisfy all EV charging demands and only the base electricity load can be shedded when they optimize their restoration plans.

Figure 9 shows the traffic-power systems performance evolution over the restoration horizon under different EV penetration levels. Table 3 shows the benefit of line switching and link reversing in terms of system performance loss, for different EV penetration levels and different decision-making environments. As shown in Figure 9, the traffic-power system performance decreases as the EV penetration increases. When EV penetration increases from 0% to 100%, the nominal total costs of the traffic-power system increases from \$773300 to \$1133009, leading to a 46.7% increase in costs. The extra charging time needed for EVs, compared to GVs refueling, and the

Table 3: Solutions under different EV penetration levels and decision environments

EV Penetration	Environments	$h_a = 1$	$u_{i,j} = 0$	Total cost ($)	Cost for RNs ($)	Cost for PNs ($)	Vehicles	GVs	EVs	Charging demand (MW)
0%	Interdependent	5,104,117	4-7,4-9,6-13	773300	729300	44000	30540	30540	0	0
	Independent	-*	4-9,7-9,13-14	773300	729300	44000	22142	30540	0	0
25%	Interdependent	5,104,117	4-7,4-9,6-13	821260.15	775340.15	45920	26933.5	25346	1587.5	166.4
	Independent	-	4-7,4-9,9-14	824392.15	770192.15	54200	21987	19656	2331	255.2
50%	Interdependent	5,104,117	4-7,4-9,6-13	894274.2	845226.2	49048	21987	19656	2331	207.68
	Independent	-	4-7,4-9,13-14	897389.5	843069.5	54320	21999.5	19656	2343.5	294
75%	Interdependent	11,109,117	4-7,4-9,6-13	994669.5	945509.5	49160	13980	11325	2655	218.4
	Independent	-	4-7,4-9,13-14	998,262	943462	54800	14430	10437	3105	318
100%	Interdependent	22,102,117	4-7,4-9	1133009	1083849	49160	2822.5	0	2822.5	210
	Independent	117	4-7,4-9,13-14	1134561.5	1081801.5	52760	3272.5	0	3272.5	243.6

* The solution is the same for the interdependent environment

limited chargers are the main reasons of this result. When the EV penetration is equal to or less than 50%, the reconfiguration solutions are stable for both the traffic-power systems and the independently optimized RN. In this situation, links 5, 104 and 117 in the RN are reversed. Lines 4-7, 4-9 and 6-13 are always switched off, when the restoration plans of the PN are coordinately optimized. When there are no EVs in the RN, both interdependent or independent plans of restoration of the RN and the PN, have the same nominal total system performance cost. When the proportion of EVs in RN increases, the nominal total costs of the interdependent plan for the traffic-power system restoration are lower than those of the independent plans. This shows the added value of coordinately operating the two networks. The difference of the total charging demand between the coordinately managed EV charging and the independently managed one is reported in the last column of Table 3 and shown in Figure 10. The charging demand in the interdependent decision-making environment is always less than that in the independent one. This leads to higher nominal loss costs in the RN and lower costs in the PN, but lower total costs for the two networks, comparing to the independent decision making. This shows that the coordinated scheduling of charging demands leads to a trade-off of performance loss between the two networks, for the studied case.

4. Conclusion

In this paper, we have formulated mathematical models for the reconfiguration process of road networks (RNs) and power networks (PNs) to minimize the system performance loss during the restoration period after disruptive events. In both networks, system performance loss has been measured by the unmet demand, i.e., cumulative unmet gasoline vehicles (GVs) and electric vehicles (EVs) traffic demand for RNs and cumulative shedded electricity load for PNs. For RNs, the proposed model was aimed to solve the system optimal dynamic traffic assignment problem considering the characteristics of EVs and fast-charging stations (FCSs). These characteristics include driving range (battery capacity) and state of charge (SoC) of EVs, and physical constraints in FCSs, such as number of chargers and charging power. Moreover, a mixed integer program model has been proposed to minimize the integrated system performance loss during the restoration period. Contraflow technique in the RN and line switches in the PN have been used as reconfiguration strategies to enhance the system resilience after a disruptive event. The dynamic interactions between the PN and RN have been considered in the proposed integrated traffic-power systems model. The two networks have been coupled through EV charging demand, which is coordinately managed in the proposed model. A partial highway network in North Carolina (NC), USA and a modified IEEE 14-bus system have been used to illustrate the proposed methods. The results have shown that: 1) applying emergency response actions (i.e., network topology control) to the coupled traffic-power networks, the system performance can be largely improved from 76.58% to

86.26%; 2) it is better to integrally plan the emergency response for the PNs and RNs, since it could reduce the system performance loss more than independently operating them; 3) the higher EV penetration leads to the lower efficiency of the RN, which hints that the number of FCSs should be well designed along the highway to guarantee a certain service level of the RNs under extreme events. The negative impacts of increasing EV penetration on RNs and PNs require further attention and investigation. The proposed models could be employed to provide effective emergency reconfiguration solutions (e.g., links reversing in RNs and lines switching in PNs) for traffic-power systems to enhance the system resilience. Operational solutions (i.e., system optimal dynamic traffic assignment and optimal power flow distribution) could serve as a benchmark to manage the traffic-power flow and EV charging demand.

For the computational efficiency, three points need to be clarified. Firstly, the computational times of the proposed methods are influenced by many factors, such as the considered time horizon, configuration of the FCSs, EV penetrations and their battery capacities. Especially, the numbers of both the lines that can be switched in the power network and of the links that can be reversed in the road network heavily influence the computational complexity. In practice, even if the whole transmission network and the highway network are really large, the lines and links that can be controlled are limited, because of regulatory policies, operational limitations, physical constraints and so on. Secondly, if there is a really high requirement for the computational time, there are two methods that can be considered to increase the computational efficiency of the proposed approaches: 1) we may increase the time interval δ for updating the state of the traffic and power flow; this can directly decrease the number of variables by reducing the set of periods, set of links and set of energy levels of EVs, leading to less memory and computational time though at the expense of less fine-grained results; 2) we can also adjust the optimality gap tolerance in the mxied integer programming (MIP) solver, which can often significantly reduce the computational time: in our cases, if we set the gap tolerance as 5%, most results can be obtained in minutes; moreover, in practice, the exact optimal solution usually is not necessary and 5% of the optimality gap tolerance is acceptable. Finally, the considered problem is a MIP problem, which is essentially NP-hard. Decomposition algorithms such as Benders decomposition can be considered to improve the computational efficiency of the proposed models in the future.

The main limitation of the proposed method is that many variables are designed to describe the dynamic state of charge of EVs, which increases the complexity of the proposed model. In the current work, these variables are used to constrain the driving ranges of EVs and calculate their charging demand at FCSs. However, their SoCs at each time interval are not necessarily known in the emergency response problem studied in the present paper. Therefore, in the future, a more efficient modeling method is worthy exploring to improve the computational efficiency.

In this work we assume that the vehicles follow the system optimal principle to take their paths. In normal situation, sophisticated economical mechanisms can be designed to make the traffic flows follow the system optimum. However, under post-disruption situation, the originally designed economical mechanism may not work any longer, since the network topology may have been changed by the disruption. Moreover, the new economical mechanism may have not been well designed or applied in times of disruption. However, in such emergency situations, authorities may guide all vehicle drivers to follow the system optimal principle in order to mitigate the disruption. Alternatively, replacing system optimality by user equilibrium in the dynamic traffic assignment problem is a potential solution to model the situation where the drivers take the paths which meet better their own benefits. But, it is challenging for the traffic-power systems model: satisfying user equilibrium conditions requires a more complicated modeling of the charging behaviors of EVs, which might result in extremely expensive computational cost.

This work can also be extended in the following two directions: 2) including mobile energy storage systems (MESSs) into the emergency response strategies could be an effective way to improve the resilience of RNs; however, how to integrate MESSs into the traffic-power system model needs more research; 3) EVs are assumed to only replenish batteries in FCS, in the present paper: the V2G technology at FCSs can be considered to more efficiently operate the coupled traffic-power systems and strengthen their resilience.

Appendix A. Data discription

A partial highway network in NC, USA is shown in Figure 6. The used parameters of this studied network are listed in Tables A.4 and A.5. The node ID, its corresponding town or city name and its population within this area are listed in Table A.6. The cities or towns connected source-sink nodes are those whose population is more than 11000. Considering their geographic distances among these nodes and their population, the gravity model is used to generate the daily traffic demand. The generic form of the gravity model [75] is usually written as $f_{od} = P_o^{\alpha} P_d^{\beta} / D_{od}^{\gamma}$, where P_o and P_d are the population sizes of origin a and destination d, respectively, D_{od} is the shortest distance between them, α, β and γ are fitting parameters. We set $\alpha = \beta = 0.92$ and $\gamma = 1$, in this study. To consider the worst-case scenario, the traffic volumes at 17:00 and 18:00 are adopted, which is the peak of traffic and accounts for approximately 15.3% of the whole daily traffic, in the basic time-of-day patterns [76]. The traffic volumes usually show the directional differences and it is difficult to get the applicable statistics for time-of-day travel by direction for each O-D pair [76]. For simplicity, only one direction is randomly selected for each O-D pair and traffic volumes in the other direction are ignored. The obtained traffic demand is shown in Table A.7.

According to Ref. [77], the electricity demand in U.S. has peak hours similar to traffic volumes, and the demand does not change a lot during this period. For simplicity, it is assumed that the base load at each bus is constant during this period and follows the standard test data [73].

Acknowledgments

The participation of Hongping Wang to this research is supported by China Scholarship Council (No. 201606990003). Enrico Zio acknowledges the financial support from the Energy for Motion Project "Dipartimenti Eccellenti 2018-2022", funded by the Italian Ministry of University and Research (MUR).

References

[1] Y.-P. Fang, G. Sansavini, Optimum post-disruption restoration under uncertainty for enhancing critical infrastructure resilience, Reliability Engineering & System Safety 185 (2019) 1–11.

[2] S. Ma, B. Chen, Z. Wang, Resilience enhancement strategy for distribution systems under extreme weather events, IEEE Transactions on Smart Grid 9 (2016) 1442–1451.

[3] C. R. Center, Post event report: Henan flood – july 17-21, https://www.gccapitalideas.com/2021/07/28/post-event-report-henan-flood-july-17-21/, 2021. Accessed August. 20, 2021.

Table A.4: Parameters of the studied highway network

Link ID	Start	End	ν_a	β_a	ρ_a	Type	$L_a k_{jam}$	f_a^I / f_a^O	Lanes
1/101	2/1	1/2	5	10	5	G	13910	500	2
2/102	2/3	3/2	3	6	3	G	8346	500	2
3/103	3/8	8/3	4	8	4	G	5564	250	1
4/104	1/5	5/1	3	6	3	G	8346	500	2
5/105	2/5	5/2	3	6	3	G	8346	500	2
6/106	2/6	6/2	3	6	3	G	8346	500	2
7/107	3/4	4/3	1	2	1	G	1391	250	1
8/108	5/6	6/5	1	2	1	G	2782	500	2
9/109	4/6	6/4	3	6	3	G	4173	250	1
10/110	4/7	7/4	2	4	2	G	2782	250	1
11/111	4/8	8/4	3	6	3	G	4173	250	1
12/112	6/7	7/6	5	10	5	G	13910	500	2
13/113	6/7	7/6	5	10	5	G	6955	250	1
14/114	7/8	8/7	2	4	2	G	5564	500	2
15/115	7/8	8/7	2	4	2	G	2782	250	1
16/116	1/10	10/1	4	8	4	G	11128	500	2
17/117	10/14	14/10	3	6	3	G	8346	500	2
18/118	5/15	14/5	5	10	5	G	6955	250	1
19/119	11/14	14/11	2	4	2	G	5564	500	2
20/120	5/9	9/5	2	4	2	G	5564	500	2
21/121	6/9	9/6	2	4	2	G	5564	500	2
22/122	9/11	11/9	2	4	2	G	5564	500	2
23/123	11/9	9/11	2	4	2	G	5564	500	2
24/124	11/12	12/11	4	4	4	G	11128	500	2
25/125	6/12	12/6	4	4	4	G	11128	500	2
26/126	12/13	13/12	3	6	3	G	4173	250	1
27/127	7/13	13/7	2	4	2	G	2782	250	1
29/129	2/201	201/2	0	0	0	S/R	inf	inf	
30/130	10/202	202/10	0	0	0	S/R	inf	inf	
36/136	5/203	203/5	0	0	0	S/R	inf	inf	
31/131	11/204	204/11	0	0	0	S/R	inf	inf	
32/132	12/205	205/12	0	0	0	S/R	inf	inf	
33/133	14/206	206/14	0	0	0	S/R	inf	inf	
34/134	8/207	207/8	0	0	0	S/R	inf	inf	
35/135	3/208	208/3	0	0	0	S/R	inf	inf	

Table A.5: Parameters of the studied traffic-power system

Parameters	Values
v_f (m/h)	65
k_{jam}(veh/m)	214
δ (min)	6
q_{max} (veh/h/lane)	2500
p_a^{ev} (kW)	80
η (kMh/mile)	0.4
ϕ ($/h)	13
C	1
E_c	10
α_a^t (ELs/δ)	3
Initial EL of EV	3

Table A.6: Population of the towns and cities

Node ID	Name	Population	Node ID	Name	Population
1	Zebulon	4526	2	Rocky Mount	56650
3	Tarboro	11255	4	Pinetops	1351
5 & 6	Wilson	49436	7	Farmville	4695
8	Greenville	86142	9	Kenly	1344
10	Raleigh	418099	11	Selma & Smithfield	17901
12	Goldsboro	35609	13	Snow Hill	1611
14	Clayton	16529			

[4] A. A. Ganin, M. Kitsak, D. Marchese, J. M. Keisler, T. Seager, I. Linkov, Resilience and efficiency in transportation networks, Science advances 3 (2017) e1701079.

[5] X. Zhang, S. Mahadevan, S. Sankararaman, K. Goebel, Resilience-based network design under uncertainty, Reliability Engineering & System Safety 169 (2018) 364–379.

[6] C. Zhu, J. Wu, M. Liu, J. Luan, T. Li, K. Hu, Cyber-physical resilience modelling and assessment of urban roadway system interrupted by rainfall, Reliability Engineering & System Safety 204 (2020) 107095.

[7] J. Kong, C. Zhang, S. P. Simonovic, Optimizing the resilience of interdependent infrastructures to regional natural hazards with combined improvement measures, Reliability Engineering & System Safety 210 (2021). doi:{10.1016/j.ress.2021.107538}.

[8] H. Wang, A. F. Abdin, Y.-P. Fang, E. Zio, Resilience assessment of electrified road networks subject to charging station failures, Computer-Aided Civil and Infrastructure Engineering (2021). doi:https://doi.org/10.1111/mice.12736.

[9] T. Aven, A risk science perspective on the discussion concerning safety I, safety II and safety III, Reliability Engineering & System Safety 217 (2022) 108077.

[10] A. Martinetti, M. M. Chatzimichailidou, L. Maida, L. van Dongen, Safety I–II, resilience and antifragility engineering: a debate explained through an accident occurring on a mobile

Table A.7: O-D pairs and their traffic demand

Link ID	Node ID	Demand	Link ID	Node ID	Demand
130	203	6460	136	204	620
129	202	5700	129	208	620
130	206	5500	133	203	460
134	202	5380	131	205	460
130	205	3720	133	204	460
131	202	3560	131	201	400
136	201	2400	134	204	380
129	207	1720	129	206	320
136	207	1520	136	208	320
134	205	1120	133	205	280
130	208	960	134	206	260
132	203	940	132	208	160
132	201	760	135	204	100
135	207	680	135	206	60

elevating work platform, International journal of occupational safety and ergonomics 25 (2019) 66–75.

[11] T. Aven, The call for a shift from risk to resilience: What does it mean?, Risk Analysis 39 (2019) 1196–1203.

[12] X. Liu, Y.-P. Fang, E. Zio, A Hierarchical Resilience Enhancement Framework for Interdependent Critical Infrastructures, Reliability Engineering & System Safety 215 (2021). doi:{10.1016/j.ress.2021.107868}.

[13] E. Ferrario, A. Poulos, S. Castro, J. C. de la Llera, A. Lorca, Predictive capacity of topological measures in evaluating seismic risk and resilience of electric power networks, Reliability Engineering & System Safety 217 (2022). doi:{10.1016/j.ress.2021.108040}.

[14] L. Sun, D. D'Ayala, R. Fayjaloun, P. Gehl, Agent-based model on resilience-oriented rapid responses of road networks under seismic hazard, Reliability Engineering & System Safety 216 (2021). doi:{10.1016/j.ress.2021.108030}.

[15] K. Paul, N. Kumar, Cuckoo search algorithm for congestion alleviation with incorporation of wind farm., International Journal of Electrical & Computer Engineering (2088-8708) 8 (2018).

[16] K. Paul, N. Kumar, S. Agrawal, K. Paul, Optimal rescheduling of real power to mitigate congestion using gravitational search algorithm, Turkish Journal of Electrical Engineering & Computer Sciences 27 (2019) 2213–2225.

[17] X. Zhang, H. Tu, J. Guo, S. Ma, Z. Li, Y. Xia, C. K. Tse, Braess paradox and double-loop optimization method to enhance power grid resilience, Reliability Engineering & System Safety 215 (2021). doi:{10.1016/j.ress.2021.107913}.

[18] K. Paul, P. Dalapati, N. Kumar, Optimal rescheduling of generators to alleviate congestion in transmission system: A novel modified whale optimization approach, Arabian Journal for Science and Engineering (2021) 1–25.

[19] K. Paul, N. Kumar, P. Dalapati, Bat algorithm for congestion alleviation in power system network, Technology and Economics of Smart Grids and Sustainable Energy 6 (2021) 1–18.

[20] T. Aziz, Z. Lin, M. Waseem, S. Liu, Review on optimization methodologies in transmission network reconfiguration of power systems for grid resilience, International Transactions on Electrical Energy Systems 31 (2021) e12704.

[21] Y. Wang, A. O. Rousis, G. Strbac, On microgrids and resilience: A comprehensive review on modeling and operational strategies, Renewable and Sustainable Energy Reviews 134 (2020) 110313.

[22] D. Fan, Y. Ren, Q. Feng, Y. Liu, Z. Wang, J. Lin, Restoration of smart grids: Current status, challenges, and opportunities, Renewable and Sustainable Energy Reviews 143 (2021) 110909.

[23] D. Braess, Über ein paradoxon aus der verkehrsplanung, Unternehmensforschung 12 (1968) 258–268.

[24] H. Glavitsch, Switching as means of control in the power system, International Journal of Electrical Power & Energy Systems 7 (1985) 92–100.

[25] H. Sekhavatmanesh, R. Cherkaoui, Distribution network restoration in a multiagent framework using a convex opf model, IEEE Transactions on Smart Grid 10 (2018) 2618–2628.

[26] H. Sabouhi, A. Doroudi, M. Fotuhi-Firuzabad, M. Bashiri, Electricity distribution grids resilience enhancement by network reconfiguration, International Transactions on Electrical Energy Systems (2021) e13047.

[27] P. Agrawal, N. Kanwar, N. Gupta, K. Niazi, A. Swarnkar, Resiliency in active distribution systems via network reconfiguration, Sustainable Energy, Grids and Networks 26 (2021) 100434.

[28] I. G. Guimaraes, D. P. Bernardon, V. J. Garcia, M. Schmitz, L. L. Pfitscher, A decomposition heuristic algorithm for dynamic reconfiguration after contingency situations in distribution systems considering island operations, Electric Power Systems Research 192 (2021) 106969.

[29] W. Li, Y. Li, C. Chen, Y. Tan, Y. Cao, M. Zhang, Y. Peng, S. Chen, A full decentralized multi-agent service restoration for distribution network with DGs, IEEE Transactions on Smart Grid 11 (2019) 1100–1111.

[30] F. Liberati, A. Di Giorgio, A. Giuseppi, A. Pietrabissa, F. D. Priscoli, Efficient and risk-aware control of electricity distribution grids, IEEE Systems Journal 14 (2020) 3586–3597.

[31] H. Sekhavatmanesh, R. Cherkaoui, Analytical approach for active distribution network restoration including optimal voltage regulation, IEEE Transactions on Power Systems 34 (2018) 1716–1728.

[32] Y. Zhang, M. Bansal, A. R. Escobedo, Risk-neutral and risk-averse transmission switching for load shed recovery with uncertain renewable generation and demand, IET Generation, Transmission & Distribution 14 (2020) 4936–4945.

[33] M. Nazemi, P. Dehghanian, Seismic-resilient bulk power grids: Hazard characterization, modeling, and mitigation, IEEE Transactions on Engineering Management 67 (2019) 614–630.

[34] N. Gholizadeh, S. H. Hosseinian, M. Abedi, H. Nafisi, P. Siano, Optimal placement of fuses and switches in active distribution networks using value-based MINLP, Reliability Engineering & System Safety 217 (2022). doi:{10.1016/j.ress.2021.108075}.

[35] P. Dalapati, K. Paul, Optimal scheduling for delay management in railway network using hybrid bat algorithm, in: Intelligent Computing in Control and Communication, Springer, 2021, pp. 91–103.

[36] Y. Wang, J. Wang, Integrated reconfiguration of both supply and demand for evacuation planning, Transportation research part E: logistics and transportation review 130 (2019) 82–94.

[37] Y. Wang, J. Wang, Measuring and maximizing resilience of transportation systems for emergency evacuation, IEEE Transactions on Engineering Management 67 (2019) 603–613.

[38] S.-W. Chiou, A traffic-responsive signal control to enhance road network resilience with hazmat transportation in multiple periods, Reliability Engineering & System Safety 175 (2018) 105–118.

[39] X. Koutsoukos, G. Karsai, A. Laszka, H. Neema, B. Potteiger, P. Volgyesi, Y. Vorobeychik, J. Sztipanovits, Sure: A modeling and simulation integration platform for evaluation of secure and resilient cyber–physical systems, Proceedings of the IEEE 106 (2017) 93–112.

[40] L. Sun, D. D'Ayala, R. Fayjaloun, P. Gehl, Agent-based model on resilience-oriented rapid responses of road networks under seismic hazard, Reliability Engineering & System Safety 216 (2021) 108030.

[41] Y. Wu, G. Hou, S. Chen, Post-earthquake resilience assessment and long-term restoration prioritization of transportation network, Reliability Engineering & System Safety 211 (2021) 107612.

[42] T. Zhao, Y. Zhang, Transportation infrastructure restoration optimization considering mobility and accessibility in resilience measures, Transportation Research Part C: Emerging Technologies 117 (2020) 102700.

[43] W. Wei, L. Wu, J. Wang, S. Mei, Network equilibrium of coupled transportation and power distribution systems, IEEE Transactions on Smart Grid 9 (2017) 6764–6779.

[44] H. Wang, Y.-P. Fang, E. Zio, Risk assessment of an electrical power system considering the influence of traffic congestion on a hypothetical scenario of electrified transportation system in new york state, IEEE Transactions on Intelligent Transportation Systems 22 (2021) 142–155.

[45] M. Nazemi, P. Dehghanian, X. Lu, C. Chen, Uncertainty-aware deployment of mobile energy storage systems for distribution grid resilience, IEEE Transactions on Smart Grid (2021).

[46] S. Lei, C. Chen, Y. Li, Y. Hou, Resilient disaster recovery logistics of distribution systems: Co-optimize service restoration with repair crew and mobile power source dispatch, IEEE Transactions on Smart Grid 10 (2019) 6187–6202.

[47] B. Taheri, A. Safdarian, M. Moeini-Aghtaie, M. Lehtonen, Distribution system resilience enhancement via mobile emergency generators, IEEE Transactions on Power Delivery 36 (2020) 2308–2319.

[48] D. Anokhin, P. Dehghanian, M. A. Lejeune, J. Su, Mobility-as-a-service for resilience delivery in power distribution systems, Production and Operations Management (2021). doi:10.1111/poms.13393.

[49] Y. Wang, Y. Xu, J. Li, C. Li, J. He, J. Liu, Q. Zhang, Dynamic load restoration considering the interdependencies between power distribution systems and urban transportation systems, CSEE Journal of Power and Energy Systems 6 (2020) 772–781.

[50] S. Yao, P. Wang, X. Liu, H. Zhang, T. Zhao, Rolling optimization of mobile energy storage fleets for resilient service restoration, IEEE Transactions on Smart Grid 11 (2019) 1030–1043.

[51] B. Li, Y. Chen, W. Wei, S. Huang, S. Mei, Resilient restoration of distribution systems in coordination with electric bus scheduling, IEEE Transactions on Smart Grid 12 (2021) 3314–3325.

[52] A. Belle, Z. Zeng, C. Duval, M. Sango, A. Barros, Modeling and vulnerability analysis of interdependent railway and power networks: Application to British test systems, Reliability Engineering & System Safety 217 (2022). doi:{10.1016/j.ress.2021.108091}.

[53] International Energy Agency (IEA), Global EV Outlook 2020, Technical Report, IEA, 2020.

[54] S. A. Adderly, D. Manukian, T. D. Sullivan, M. Son, Electric vehicles and natural disaster policy implications, Energy Policy 112 (2018) 437–448.

[55] K. Feng, N. Lin, S. Xian, M. V. Chester, Can we evacuate from hurricanes with electric vehicles?, Transportation research part D: transport and environment 86 (2020) 102458.

[56] S. Lei, C. Chen, Y. Song, Y. Hou, Radiality constraints for resilient reconfiguration of distribution systems: Formulation and application to microgrid formation, IEEE Transactions on Smart Grid 11 (2020) 3944–3956.

[57] D. Anokhin, P. Dehghanian, M. A. Lejeune, J. Su, Mobility-as-a-service for resilience delivery in power distribution systems, Production and Operations Management 30 (2021) 2492–2521.

[58] E. Miller-Hooks, X. Zhang, R. Faturechi, Measuring and maximizing resilience of freight transportation networks, Computers & Operations Research 39 (2012) 1633–1643.

[59] Y.-P. Fang, E. Zio, An adaptive robust framework for the optimization of the resilience of interdependent infrastructures under natural hazards, European Journal of Operational Research 276 (2019) 1119–1136.

[60] D. Valcamonico, G. Sansavini, E. Zio, Cooperative co-evolutionary approach to optimize recovery for improving resilience in multi-communities, Reliability Engineering & System Safety 197 (2020) 106800.

[61] F. He, Y. Yin, S. Lawphongpanich, Network equilibrium models with battery electric vehicles, Transportation Research Part B: Methodological 67 (2014) 306–319.

[62] A. K. Ziliaskopoulos, A linear programming model for the single destination system optimum dynamic traffic assignment problem, Transportation science 34 (2000) 37–49.

[63] F. Zhu, S. V. Ukkusuri, A cell based dynamic system optimum model with non-holding back flows, Transportation Research Part C: Emerging Technologies 36 (2013) 367–380.

[64] J. Long, W. Y. Szeto, Link-based system optimum dynamic traffic assignment problems in general networks, Operations Research 67 (2019) 167–182.

[65] I. Yperman, The link transmission model for dynamic network loading, Ph.D. thesis, KU Leuven, 2007.

[66] G. F. Newell, A simplified theory of kinematic waves in highway traffic, part i: General theory, Transportation Research Part B: Methodological 27 (1993) 281–287.

[67] G. F. Newell, A simplified theory of kinematic waves in highway traffic, part ii: Queueing at freeway bottlenecks, Transportation Research Part B: Methodological 27 (1993) 289–303.

[68] X. Zhang, S. Mahadevan, K. Goebel, Network reconfiguration for increasing transportation system resilience under extreme events, Risk analysis 39 (2019) 2054–2075.

[69] A. J. Conejo, J. A. Aguado, Multi-area coordinated decentralized D optimal power flow, IEEE transactions on power systems 13 (1998) 1272–1278.

[70] M. Woodard, K. Marashi, S. S. Sarvestani, A. R. Hurson, Survivability evaluation and importance analysis for cyber–physical smart grids, Reliability Engineering & System Safety 210 (2021) 107479.

[71] K. Marashi, S. S. Sarvestani, A. R. Hurson, Identification of interdependencies and prediction of fault propagation for cyber–physical systems, Reliability Engineering & System Safety 215 (2021) 107787.

[72] U. Washington, Power systems test case archive, http://labs.ece.uw.edu/pstca/pf14/pg_tca14bus.htm, 2021. Accessed August. 13, 2021.

[73] Y. Fang, G. Sansavini, Optimizing power system investments and resilience against attacks, Reliability Engineering & System Safety 159 (2017) 161–173.

[74] G. company, The studied highway network, https://www.google.com/maps/place/North+Carolina/@35.7432238,-78.158401,9.79z/data=!4m5!3m4!1s0x88541fc4fc381a81:0xad3f30f5e922ae19!8m2!3d35.600369!4d-78.999939, 2022. Accessed Jan. 8, 2022.

[75] Y. Ren, M. Ercsey-Ravasz, P. Wang, M. C. González, Z. Toroczkai, Predicting commuter flows in spatial networks using a radiation model based on temporal ranges, Nature communications 5 (2014) 1–9.

[76] M. Hallenbeck, M. Rice, B. Smith, C. Cornell-Martinez, J. Wilkinson, Vehicle volume distributions by classification, Technical Report, Washington State Transportation Center, 1997.

[77] U. E. I. Administration, Hourly electric grid monitor, https://www.eia.gov/electricity/gridmonitor/dashboard/electric_overview/US48/US48, 2021. Accessed August. 14, 2021.

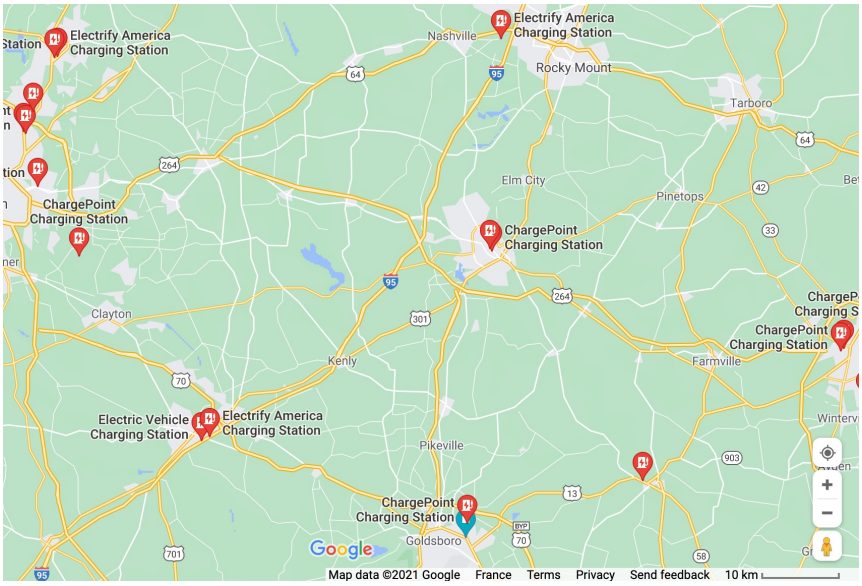

(a) The partial highway network in NC

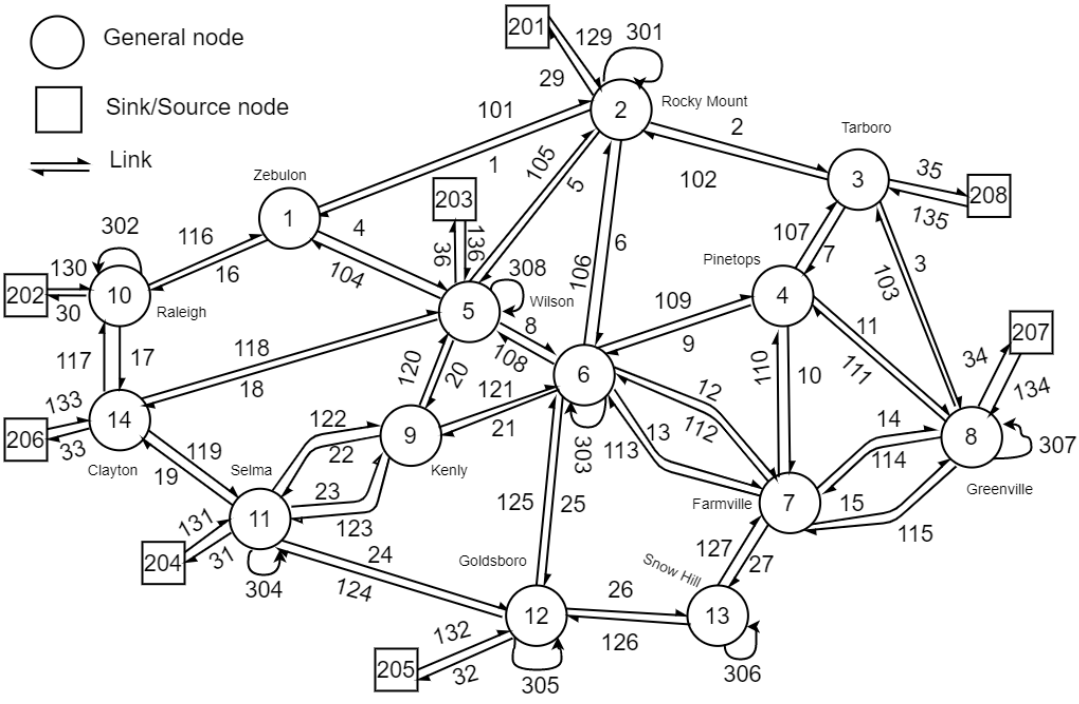

(b) The approximated topology network

Figure 6: The studied highway network [74]

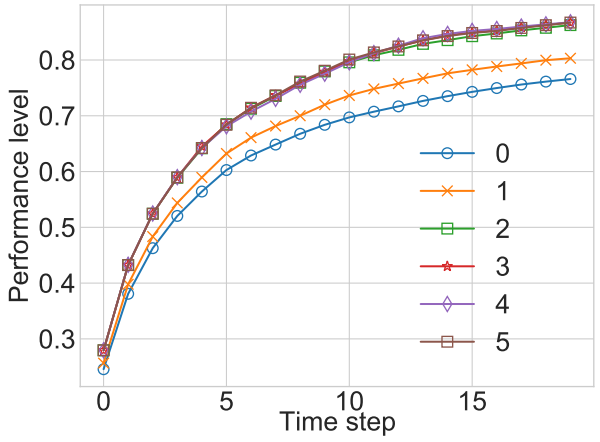

Figure 7: System performance evolution over restoration horizon under different resource level

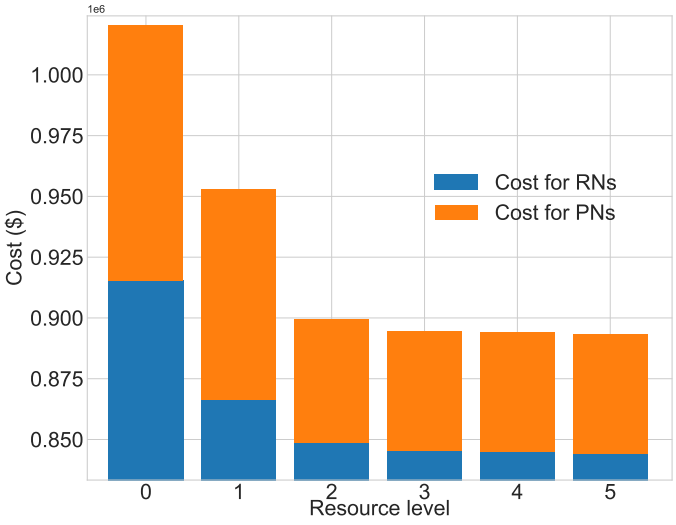

Figure 8: Nominal cost for the studied traffic-power systems under different resource level

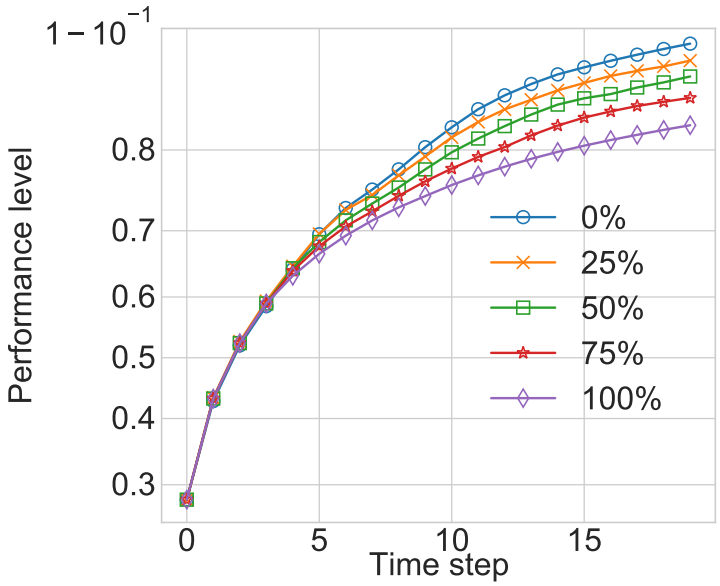

Figure 9: The traffic-power systems performance evolution over restoration horizon under different EV penetration levels

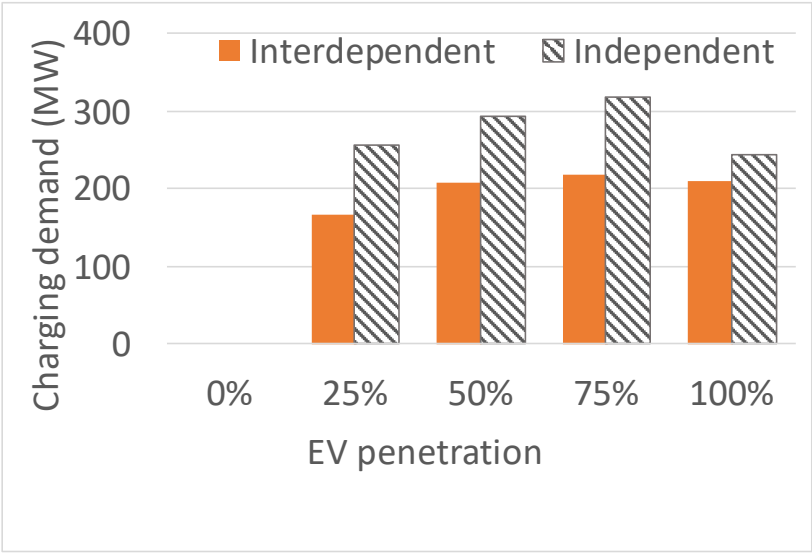

Figure 10: EV charging demand under different EV penetration levels and decision environments